MOLECULAR AND CELLULAR BIOLOGY, Sept. 1996, p. 4897–4914 Vol. 16, No. 9
0270-7306/96/$04.00+0


# The EH-Domain-Containing Protein Pan1 Is Required for Normal Organization of the Actin Cytoskeleton in *Saccharomyces cerevisiae*

HSIN-YAO TANG AND MINGJIE CAI*

*Institute of Molecular and Cell Biology, National University of Singapore, Singapore 0511, Singapore*

Received 30 April 1996/Returned for modification 7 June 1996/Accepted 24 June 1996

**Normal cell growth and division in the yeast *Saccharomyces cerevisiae* involve dramatic and frequent changes in the organization of the actin cytoskeleton. Previous studies have suggested that the reorganization of the actin cytoskeleton in accordance with cell cycle progression is controlled, directly or indirectly, by the cyclin-dependent kinase Cdc28. Here we report that by isolating rapid-death mutants in the background of the Start-deficient *cdc28-4* mutation, the essential yeast gene *PAN1*, previously thought to encode the yeast poly(A) nuclease, is identified as a new factor required for normal organization of the actin cytoskeleton. We show that at restrictive temperature, the *pan1* mutant exhibited abnormal bud growth, failed to maintain a proper distribution of the actin cytoskeleton, was unable to reorganize actin the cytoskeleton during cell cycle, and was defective in cytokinesis. The mutant also displayed a random pattern of budding even at permissive temperature. Ectopic expression of *PAN1* by the *GAL* promoter caused abnormal distribution of the actin cytoskeleton when a single-copy vector was used. Immunofluorescence staining revealed that the Pan1 protein colocalized with the cortical actin patches, suggesting that it may be a filamentous actin-binding protein. The Pan1 protein contains an EF-hand calcium-binding domain, a putative Src homology 3 (SH3)-binding domain, a region similar to the actin cytoskeleton assembly control protein Sla1, and two repeats of a newly identified protein motif known as the EH domain. These findings suggest that Pan1, recently recognized as not responsible for the poly(A) nuclease activity (A. B. Sachs and J. A. Deardorff, erratum, Cell 83:1059, 1995; R. Boeck, S. Tarun, Jr., M. Rieger, J. A. Deardorff, S. Muller-Auer, and A. B. Sachs, J. Biol. Chem. 271:432–438, 1996), plays an important role in the organization of the actin cytoskeleton in *S. cerevisiae.***

Cellular morphogenesis has been a long-standing research interest for biologists (26, 57). One of the key factors involved in cellular morphogenesis is the organization of the actin cytoskeleton. Perhaps no other organisms manifest more vividly than the yeast *Saccharomyces cerevisiae* the significance of actin cytoskeleton to cellular function and reproduction. *S. cerevisiae* cells reproduce by polarized growth, or budding, which requires the actin cytoskeleton on the cortex (known as cortical actin patches) to undergo dramatic reorganization in accordance with different stages of cell growth throughout the cell cycle (22, 34, 37, 38). The cortical actin cytoskeleton in *S. cerevisiae*, therefore, is a very dynamic structure. $G_1$ cells that have not yet passed a cell cycle stage called Start distribute their cortical actin cytoskeleton randomly in order to grow isotropically. Cell cycle progression through Start occurs in late $G_1$ and is dependent on the activity of Cdc28, a cyclin-dependent kinase, in complex with the Cln type of cyclins. Shortly after Start, the cortical actin patches polarize to a small region underneath the plasma membrane. This step sets a transition of the growth mode from isotropic to apical, since all of the efforts that cells make for growth, in the form of secretory vesicles, will be channeled to the bud site and, later, into the bud. The cortical actin patches remain at the tip of the bud during the initial phase of bud growth with few or no actin patches left inside the mother. The growth pattern in the bud shifts some time later in the budding phase from apical to isotropic, by reorganizing the cortical actin patches from the tip of the bud to even distribution inside the bud. This apical/isotropic switch, permitting the bud to grow into a spherical shape, is thought to be triggered by the activity of Cdc28 in complex with $G_2$ cyclins (Clb1 and Clb2) (37, 38), and may also require the function of the Clb2-interacting protein Nap1 (33). At the time corresponding to mitosis, cortical actin structures undergo another redistribution, first becoming evenly spread over mother and bud, then followed quickly by congregation on both sides of the neck. The latter step is a prerequisite for cytokinesis and probably requires the inactivation of the Cdc28/Clb complex (37, 38). Although Cdc28 kinase is implicated in regulation of the actin cytoskeleton network, its direct cytoskeletal targets have not yet been identified. Screening for genes required for viability in cells that had been crippled in Cdc28 kinase activity has led to the identification of several factors, such as Slt2, Cla2, and Cla4, that are found to be involved in polarized growth, cytoskeleton organization, and cytokinesis (7, 18, 19, 41). Conceivably, studies of these factors will provide more insights into the regulation of cytoskeleton organization by Cdc28. In this report, we describe the identification of a new factor required for normal organization of the actin cytoskeleton in *S. cerevisiae* by a similar screening method. By isolating mutants that lose viability rapidly in combination with a Start-deficient mutation (*cdc28-4*) at restrictive temperature, we obtained a yeast mutant, *pan1*, that exhibited various defects in the organization of the actin cytoskeleton. Genetic and molecular studies showed that the Pan1 protein plays an important role in actin cytoskeleton organization in *S. cerevisiae.*

* Corresponding author. Mailing address: Institute of Molecular and Cell Biology, National University of Singapore, 10 Kent Ridge Crescent, Singapore 0511, Singapore. Phone: (65) 7723382. Fax: (65) 7791117. Electronic mail address: mcbcaimj@leonis.nus.sg.

TABLE 1. Yeast strains

| Strain | Relevant genotype | Reference |
|---|---|---|
| US100 | *MAT***a** *cdc28-4* | 56 |
| US52 | *MAT***a** *cdc28-1N* | 56 |
| YNN413 | *MAT***a**/α *ade2/ade2 his3/his3 leu2/leu2 trp1/trp1 ura3/ura3* | 9 |
| YMW1 | *MAT*α *ade2 ade3 his3 leu2 trp1 ura3* | This study |
| YMW2 | *MAT***a** *ade2 ade3 his3 leu2 trp1 ura3* | This study |
| YMC387 | *MAT***a** *pan1-4* | This study |
| YMC388 | *MAT***a** *cdc28-4 pan1-4* | This study |
| YMC389 | *MAT***a** *cdc28-1N pan1-4* | This study |
| YMC392 | YMW2::pMC213(*GAL-PAN1 CEN6*) | This study |
| YMC393 | YMW2::pMC214(*GAL-PAN1* 2μm) | This study |
| YMC394 | YMW2::pMC215(*GAL* 2μm) | This study |
| YMC395 | *MAT***a** *pan1*Δ::*HIS3* pMC216(*GAL-HA-PAN1 CEN6*) | This study |
| YMC396 | *MAT***a**/α *pan1-4/pan1-4* | This study |
| YMC397 | *MAT***a**/α *pan1-4/PAN1 sla1*Δ::*HIS3/SLA1* | This study |
| YMC398 | *MAT***a** *pan1*Δ::*HIS3* pMC213(*GAL-PAN1 CEN6*) | This study |

## MATERIALS AND METHODS

**Strains, media, and genetic techniques.** The yeast strains used in this work are listed in Table 1. Rich medium (YPD) contained 1% yeast extract, 2% peptone, and 2% glucose. Minimal, synthetic complete (SC), and dropout media were prepared as described previously (50). SC-Leu was SC but lacked leucine and was supplemented as indicated with 2% of glucose (SC-Leu Glu), raffinose (SC-Leu Raf), or galactose (SC-Leu Gal). Restriction enzymes, ligase, and all other DNA-modifying enzymes were from either New England Biolabs or Amersham. Wild-type cells were grown at 30°C. Temperature-sensitive mutants were propagated at the permissive temperature of 23°C and analyzed at the restrictive temperature of 37°C, unless indicated otherwise. Genetic manipulations were performed according to standard methods described by Rose et al. (50). The lithium acetate method (31) was used in yeast transformation. DNA manipulations were performed as described by Sambrook et al. (53). Electrotransformation of bacterial cells was done on a GenePulser (Bio-Rad) with XL1-Blue as the host *Escherichia coli* strain (Stratagene). PCR was performed with Vent polymerase (New England Biolabs) as recommended by the manufacturer. DNA was sequenced by using Sequenase (U.S. Biochemicals), and sequences were compared to the GenBank database by using the BLAST server at the National Center for Biotechnology Information (National Institutes of Health, Bethesda, Md.).

**Isolation of mutants.** The strain US100 (*cdc28-4*) was obtained from U. Surana (56) and mutagenized with ethyl methanesulfonate (EMS) to 60% lethality. After being grown on YPD plates at a density of about 500 colonies per plate at 23°C, the colonies were replica plated onto fresh YPD plates which were then incubated at 37°C for 7 h before being allowed to grow at 23°C. The replica-plated colonies that grew poorly, if at all, on the 37°C-treated plates were selected from the master plates and tested once again for the rapid-death-at-37°C phenotype. Fifteen out of 50,000 colonies screened were confirmed to die rapidly at 37°C. Each of the rapid-death mutants was transformed with pMC186, a centromere plasmid carrying the wild-type *CDC28* gene, and reexamined for the rapid-death phenotype by comparing with the parental strain US100. Good viability was restored in two of these mutants after they acquired the *CDC28* gene and the rest showed little or no difference in their viability at 37°C. Both mutants were found to be temperature sensitive by themselves after they were crossed to a wild-type strain isogenic to US100. One of them, named YMC387 (*pan1-4*), was analyzed in this study.

**Viability and cell morphology.** Appropriate yeast strains were grown to ~$10^6$ cells per ml ($A_{600}$ = 0.5) in liquid YPD at 23°C before being shifted to 37°C. Aliquots of cells were taken at various time points for further analysis. In viability studies, cells were plated onto YPD plates and allowed to form colonies for 4 days at 23°C. Aliquots of cells from the same cultures were fixed with formaldehyde (3.7%), and the number of cells per milliliter was determined with a hemocytometer. Percentage of viability was determined by dividing the number of colonies on the YPD plates by the total number of cells that were plated. In morphology studies, cells were fixed in formaldehyde, sonicated to disrupt clumps, and analyzed with a phase-contrast microscope.

**Fluorescence studies.** Procedures used for fluorescence microscopy have been described previously (2, 34). Briefly, cells were grown in liquid culture in the conditions described and fixed by the addition of formaldehyde directly to the culture to a final concentration of 3.7%. After 10 min, cells were collected by brief centrifugation and resuspended in KPi buffer (0.1 M $KH_2PO_4$, pH 6.4) plus 3.7% of formaldehyde. Cells were collected after 60 min, washed three times in KPi, and resuspended in KPi plus 1.2 M sorbitol; however, to visualize the influenza virus hemagglutinin (HA)-tagged Pan1, cells were collected after 30 min and washed. Cellular DNA was visualized by staining with 4′,6-diamidino-2-phenylindole (DAPI; Sigma). Actin was visualized by staining with rhodamine-phalloidin (Molecular Probes Inc.). To label chitin, cells were stained with 1 μg of Calcofluor (Fluorescent Brightener 28; Sigma) per ml for 5 min and then washed five times in distilled water.

For indirect immunofluorescence, fixed and washed cells were permeabilized by incubation with 10 μg of Zymolyase 100T (ICN Biomedicals, Inc.) per ml for 60 min at 30°C. After incubation, the cells were washed once with KPi–1.2 M sorbitol, and resuspended in the same solution. Then, 10 μl of the cell suspension was transferred to a polylysine-coated well on a multiwell slide. After 1 min, the suspension was removed and the slide was immersed in −20°C methanol for 6 min and −20°C acetone for 30 s. The slide was air dried and incubated with the relevant primary antibodies followed by the secondary antibodies and subsequent antibodies if needed. All antibodies were diluted in phosphate-buffered saline (PBS) containing 1 mg of bovine serum albumin (BSA) per ml (PBS-BSA) and incubated for 60 min each, followed by four PBS-BSA washes. Slides were then mounted in 90% glycerol containing *p*-phenylenediamine. To visualize microtubule structures, the rat monoclonal YOL1/34 (Serotec) antibody was used as the primary antiserum and rhodamine-conjugated goat anti-rat immunoglobulin G (IgG) (Jackson ImmunoResearch) was used as the secondary antibody. Actin was visualized by using guinea pig anti-actin (a gift of D. Botstein, Stanford University, Stanford, Calif.) and fluorescein-conjugated donkey anti-guinea pig IgG (Jackson ImmunoResearch). The HA-Pan1 was visualized by using mouse monoclonal antibody 12CA5 (Boehringer Mannheim), which recognizes the HA epitope, and rhodamine-conjugated goat anti-mouse IgG (Jackson ImmunoResearch). To costain HA-Pan1 and actin, the antibodies were used in the following order: mouse anti-HA, guinea pig anti-actin, rhodamine-conjugated goat anti-mouse IgG, and finally fluorescein-conjugated donkey anti-guinea pig IgG. In control experiments, no cross-reactivity was observed between mouse anti-HA and fluorescein-conjugated donkey anti-guinea pig IgG, between guinea pig anti-actin and rhodamine-conjugated goat anti-mouse IgG, or between rhodamine-conjugated goat anti-mouse IgG and fluorescein-conjugated donkey anti-guinea pig IgG. All cells were observed and photographed with a Zeiss Axioplan microscope.

**Measurement of DNA content of yeast cells.** At each time point, cells were fixed with 70% ethanol for 1 h or overnight at 4°C. Cells were then washed with water and resuspended in 0.1 ml of 10 mM Tris-HCl (pH 8.0)–10 mM NaCl–50 μg of propidium iodide per ml–1 mg of RNase A per ml for 4 h at 37°C. Stained cells were subsequently diluted into 1 ml of PBS, and, for each sample, the DNA content of 10,000 cells was determined with a FACScan flow cytometer (Becton Dickinson).

**Cloning of *PAN1*.** The *pan1-4* mutant (YMC387) cells were transformed with a low-copy-number YCp50 yeast genomic library (49), and the transformants were screened for plasmid-dependent growth at 37°C. Five $Ura^+$ $Ts^+$ transformants were analyzed. Upon recovery from *E. coli*, all five could retransform YMC387 to $Ura^+$ $Ts^+$. Restriction digestion indicated that all five plasmids contained overlapping regions of DNA. Various parts of the insert from a plasmid containing a 7-kb *Eco*RI fragment were subcloned into yeast centromere plasmid pRS315 (55) for further analysis. The smallest complementing fragment was localized to a 2.4-kb *Eco*RI-*Pst*I fragment (see Fig. 6A). Sequence analysis revealed that this fragment was identical to the previously described *PAN1* gene (52). Subsequently, the plasmid pHT837, containing the complete *PAN1* gene on the 5.8-kb *Bam*HI (blunted)-*Eco*RI fragment (see Fig. 6A), was used for all experiments requiring the wild-type gene.

To construct the *PAN1* gene under the control of the *GAL1* promoter, an *Eco*RI site was first created in front of the ATG start codon by PCR. The 1.2-kb PCR product, extending from the start codon to the next *Eco*RI site, was digested with *Eco*RI and ligated to a vector containing the *GAL1* promoter. The resulting plasmid with the *Eco*RI fragment in the correct orientation was digested with *Msc*I-*Not*I (blunted) to remove most of the PCR-generated *PAN1* and replaced with the *Msc*I-*Kpn*I (blunted) fragment of the wild-type *PAN1* gene. Both *Not*I and *Kpn*I sites are from the multiple cloning site of the vector. The complete *GAL-PAN1* was then excised by *Pvu*I digestion and cloned into *Pvu*I-digested pRS315 and pRS425 (13) to generate pMC213 and pMC214, respectively.

**Integration mapping and gene disruptions.** To confirm that the cloned DNA represents the authentic *PAN1* gene, the 3.8-kb *Eco*RI fragment containing the 5′ truncated *PAN1* gene was cloned into the *Eco*RI site of the *URA3*-containing integrating vector pRS306 (55). The resulting plasmid was cleaved within the *PAN1* gene at the unique *Nhe*I site and used to transform a wild-type haploid strain YMW1 to uracil prototrophy. The structure of this genomic integration was confirmed by Southern hybridization. The resultant haploid strain was crossed to YMC387 (*pan1-4*), and the diploid was sporulated. A total of 30 tetrads were dissected, and all segregated as 2 $Ura^+$ $Ts^+$:2 $Ura^-$ $Ts^-$.

The *PAN1* gene was disrupted by the one-step gene replacement method (51). pHT837 was digested with *Msc*I-*Bam*HI to remove most of the *PAN1* sequences, and a 1.4-kb *Bam*HI-*Eco*RV fragment containing the *HIS3* gene was cloned into it. This leaves 287 and 143 nucleotides from the 5′ and from the 3′ coding sequences of *PAN1*, respectively. The *HIS3* gene together with *PAN1* flanking sequences (*pan1*Δ::*HIS3*) was then excised by *Eco*RI, gel purified, and transformed into a wild-type diploid strain, YNN413. The deletion was confirmed by

Southern hybridization. When sporulated and dissected, this diploid *pan1*Δ strain produced only two viable spores.

To create the *sla1* deletion strain, the complete *SLA1* gene (accession no. Z22810) was first obtained from the yeast genome by PCR. This fragment, extending from nucleotides 50 to 4391 of the database sequence, was cloned into the vector pBluescript KSII$^+$ (Stratagene). The resulting plasmid was then digested with *Msc*I and *Xba*I (blunted) to remove most of the coding region of *SLA1*, and a 1.4-kb *Bam*HI (blunted)-*Xho*I (blunted) *HIS3* fragment was cloned into it. This *sla1*Δ construct has 64 and 4 nucleotides of the *SLA1* coding sequence remaining at the 5′ and 3′ ends, respectively. The construct together with *SLA1* flanking sequences was excised by digesting with *Xho*I-*Sac*II on the polylinker, gel purified, and transformed into a wild-type haploid strain YMW1. The deletion was then confirmed by Southern hybridization. The resultant strain was crossed to YMC387 (*pan1-4*) to generate the heterozygous diploid YMC397 (*Mat***a**/α *pan1-4*/*PAN1 sla1*Δ::*HIS3*/*SLA1*).

**Epitope tagging, protein extraction, and cellular fractionation of *Pan1*.** For tagging Pan1 at the N terminus, PCR was used to generate a unique *Asp*718 (Boehringer Mannheim) site after the initiation codon in the plasmid pMC213 (*GAL-PAN1*). Subsequently, an *Asp*718 cassette containing three tandem repeats of the HA epitope (YPYDVPDYAG) was inserted in frame to generate the *GAL-HA-PAN1* construct. This construct was then moved into the vector pRS316 by *Pvu*I digestion to generate the plasmid pMC216.

Two truncated versions of pMC216 were generated to confirm the HA-Pan1 construct. The HA-Pan1Δ1208-1480 was generated by removing the *PAN1* DNA sequence downstream of the *Pst*I site in pMC216. This generates a deletion from amino acid 1208 to 1480 but includes 27 amino acids due to the translation of the polylinker sequences before a stop codon is encountered. The HA-Pan1Δ1055-1480 was generated similarly by removing the sequences downstream of the *Xho*I site. This generates a deletion from amino acid 1055 to 1480 but includes 14 amino acids from the polylinker.

To obtain crude extracts from various yeast strains, the cells were grown under selective conditions to mid-log phase ($A_{600}$ = 0.9 to 1.2). Cells were harvested, washed once in stop mixture (0.9% NaCl, 1 mM $NaN_3$, 10 mM EDTA, 50 mN NaF), and then resuspended in 0.2 ml of ice-cold lysis buffer (1% Triton X-100, 1% sodium deoxycholate, 0.1% sodium dodecyl sulfate [SDS], 50 mM Tris-HCl [pH 7.2], 0.1 mM sodium orthovanadate, 1 mM phenylmethylsulfonyl fluoride, and protease inhibitors). Cells were then lysed at 4°C by vortexing with 400- to 500-μm acid-washed glass beads. After centrifugation, loading buffer was added to the cell lysate and the mixture was analyzed by SDS-polyacrylamide gel electrophoresis (SDS-PAGE).

Cell fractionation experiments were based on methods described by Kuchler et al. (36). Briefly, yeast strain YMC395 cells containing the *GAL-HA-PAN1* gene (pMC216) were grown under selective conditions in 2% galactose to mid-exponential phase ($A_{600}$ = 0.9 to 1.2). Cells were harvested, washed once, and resuspended in 0.5 ml of ice-cold lysis buffer (10 mM Tris-HCl, 1 mM EDTA [pH 7.8], containing 2% 2-mercaptoethanol, 1 mM phenylmethylsulfonyl fluoride, and protease inhibitors). Cells were then lysed at 4°C by vortexing with 400- to 500-μm acid-washed glass beads. The resulting cell lysate was diluted 5- to 10-fold with lysis buffer, and unbroken cells, glass beads, and large debris were removed by centrifugation at 300 × *g* for 5 min at 4°C. The 300 × *g* supernatant (S1) was then spun at 10,000 × *g* for 10 min at 4°C, and the pellet (P2) was resuspended in the same volume of lysis buffer. Finally, the 10,000 × *g* supernatant (S2) was spun at 100,000 × *g* for 1 h at 4°C, producing the third supernatant (S3) and pellet (P3) which was resuspended in the same volume of lysis buffer. To assess the relative amount of Pan1 in each fraction, equal volumes of each fraction were loaded onto an SDS-PAGE gel (7.5% polyacrylamide). The resolved proteins were electrotransferred to an Immobilon-P membrane (Millipore) according to instructions provided by the manufacturer (Bio-Rad). The HA-tagged Pan1 protein was subsequently detected by using anti-HA antibody (clone 12CA5; Boehringer Mannheim) and horseradish peroxidase-conjugated goat anti-mouse IgG secondary antibody. Antibody-antigen complexes were visualized with the ECL system (Amersham).

To determine the nature of the interaction between Pan1 and the particulate fraction, the 10,000 × *g* pellet was resuspended in 10% glycerol–1 mM EDTA–50 mM Tris-HCl (pH 7.8)–10 mM $MgCl_2$. Equal portions were then treated with one of the following reagents: 1% SDS, 1% Triton X-100, 0.1 M $Na_2CO_3$ (pH 11), 2 M urea, or water as a control. After 1 h at 4°C, each mixture was spun at 10,000 × *g* for 10 min. Each pellet was resuspended in the same volume as the supernatant. All samples were then analyzed by Western blotting (immunoblotting).

## RESULTS

**Isolation of mutants that died rapidly in combination with *cdc28-4*.** Start is the initiation point of the yeast cell cycle and requires the function of Cdc28 (48). Passage through Start is a prerequisite for budding, DNA synthesis, and other events necessary for cell division and is under strict control by growth-related factors such as cell size and nutritional supplies (43). In order to gain more insight into the control of Start, we attempted the isolation of mutants that could undergo rapid death in the presence of the *cdc28-4* mutation at the restrictive temperature of 37°C. The *cdc28-4* mutant arrests preferentially at Start, before bud emergence and DNA synthesis (48). Although arrested in cell cycle progression, the *cdc28-4* cells incubated at 37°C are still able, within a limited period of time, to maintain normal rates of protein and RNA synthesis, continue to grow in size, and remain viable after temperature down-shift (48). We reasoned that perturbation of the cell cycle arrest in *cdc28-4* cells due to additional mutations may result in a rapid-death phenotype at 37°C, and mutations that could interfere with the cell cycle arrest of *cdc28-4* may define genes that are required for proper control of the Start events.

From a total of 50,000 EMS-mutagenized colonies, 15 mutants that died rapidly at 37°C were isolated. To distinguish the mutants that would die rapidly only when combined with the *cdc28-4* mutation from those whose rapid-death phenotype was irrespective of *cdc28-4*, these mutants were transformed with the wild-type *CDC28* gene carried on a centromere plasmid. Thirteen of them still exhibited rapid death at 37°C in the presence of the *CDC28* gene and were therefore discarded. The other two mutants that regained viability for 37°C treatment and yet remained temperature sensitive after they acquired *CDC28* were back-crossed to an isogenic wild-type strain. One of the mutants, named *pan1-4* (see below), was the subject of this study.

*pan1-4* was a recessive temperature-sensitive allele. The mutant grew well at 23°C but could not survive when incubated at 37°C. It did, however, show good viability if the incubation at 37°C was limited to just a few hours, comparable to that of the *cdc28-4* mutant (Fig. 1A). The *pan1-4* mutation was back-crossed into *cdc28-4* (US100 [Table 1]) again to examine its effects on the *cdc28-4* mutant's viability and cell cycle arrest at restrictive temperature. The double mutant, though growing well at 23°C, could not withhold its viability at 37°C and died rapidly (less than 0.1% of the cells were viable after 8 h of temperature shift, compared to about 50% for the single mutants) (Fig. 1A). Moreover, the double mutant could not survive at 30°C, a semi-permissive temperature for both single mutants (Fig. 1B). If the steep drop of viability at 37°C and/or synthetic lethality at 30°C in the double mutant was specific to $G_1$-arrested cells, one could predict that another mutant allele of *CDC28*, *cdc28-1N*, which conferred cell cycle arrest at $G_2$/M rather than Start (56), may not constitute synthetic lethality with *pan1-4*. Indeed, as shown in Fig. 1B, the *cdc28-1N pan1-4* double mutant could survive well at 30°C. Similarly, the double mutants formed between *pan1-4* and each of the *cdc* mutants, *cdc9*, *cdc13*, and *cdc15*, which were arrested at cell cycle stages well after Start (48), displayed neither a significant decline in viability at 37°C compared with the *cdc* single mutants (data not shown) nor synthetic lethality at 30°C (except for *cdc13*, which as a single mutant could not survive at 30°C; data not shown). These data suggested that *pan1-4* may cause lesions more hazardous to cells that are defective in cell cycle progression through $G_1$ than that defective in other stages of cell cycle.

Although the *pan1-4* mutation had a dramatic effect on the cell viability of the *cdc28-4* mutant, it did not enable *cdc28-4* cells to escape from being arrested as unbudded cells with 1 N content of DNA at 37°C (see below).

**Phenotypic characterization of the *pan1-4* mutant.** At the permissive temperature of 23°C, the morphology of *pan1-4* cells, as judged by phase-contrast microscopy, resembled the isogenic wild-type cells except for the occasional appearance of two-budded cells (less than 5% of the population) which were more prominent at 37°C (Fig. 2A, left). Transfer of asynchronous cultures of the *pan1-4* mutant from 23 to 37°C led to a rapid increase in the population of budded cells. Within 2 h of

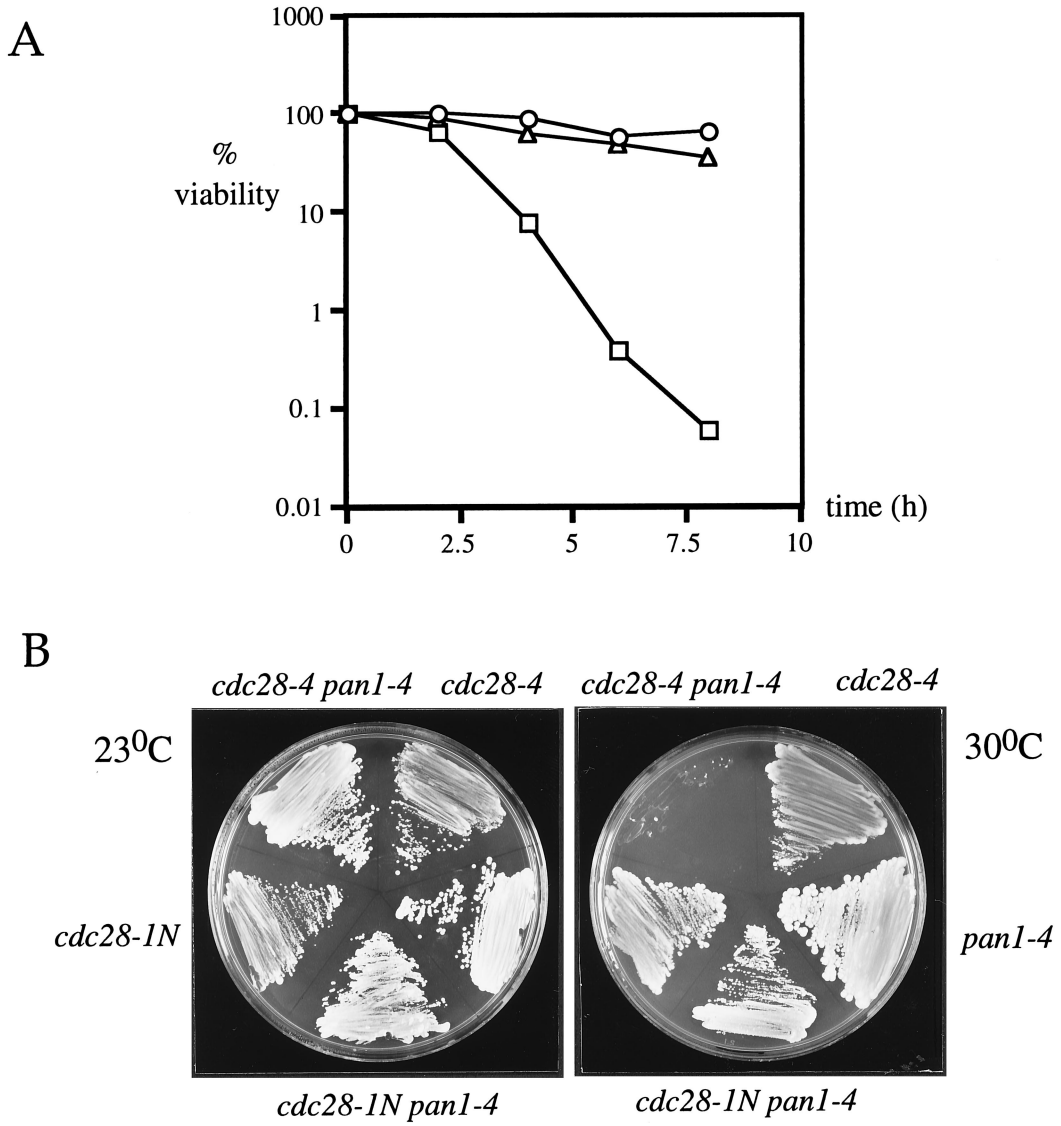


FIG. 1. Viability of *pan1-4*, *cdc28-4*, and *cdc28-1N* mutants. (A) Log-phase cells of US100 (*cdc28-4* [○]), YMC387 (*pan1-4* [△]), and YMC388 (*cdc28-4 pan1-4* [□]) grown at the permissive temperature of 23°C were shifted to the restrictive temperature of 37°C in liquid YPD. Cell viability was determined as described in Materials and Methods. (B) *pan1-4* and *cdc28-4* are synthetic lethal at 30°C. Photographs of US100 (*cdc28-4*), US52 (*cdc28-1N*), YMC387 (*pan1-4*), YMC388 (*cdc28-4 pan1-4*), and YMC389 (*cdc28-1N pan1-4*) strains plated on YPD and incubated for 5 days at 23 and 30°C.

temperature shift, 75% or more of the cells were at the stage of having either small buds or large buds. It became immediately evident that many of these buds were formed aberrantly because they were either elongated or growing out of two sites on the mother cells (Fig. 2A, right). Some (around 10% of the total population) of the two-budded cells had the two buds both in very small size. The total number of cells did not double within the time course of the experiment. Upon further incubation at 37°C, about 30% of the budded population underwent another round of budding with buds emerged from tips of both mother and daughter while they were still attached to each other. Treatment with glusulase could not break these cells apart (data not shown), indicating that they arose from failed cytokinesis. Morphologically, therefore, the *pan1-4* mutant cells did not appear to be uniformly arrested at a specific cell cycle stage at restrictive temperature. The flow cytometry analysis indicated that most mutant cells contained either 2 or 4 N DNA content (Fig. 2B). This profile remained unchanged till the end of the time course (up to 10 h). Fluorescence staining of the mutant cells with DAPI and anti-tubulin antibody displayed a heterogeneous pattern of nuclear and microtubule structures (Fig. 2C). DAPI staining also revealed a fraction of cells (about 20%) undergoing nuclear division within the mother cells resulting in binucleate cells (Fig. 2C). This suggested that spindle orientation or nuclear migration might be also defective in the *pan1-4* mutant.

The above phenotypes of the *pan1-4* mutants were confirmed by using cells synchronized in $G_1$ by nutrient depletion before being shifted to 37°C. The *pan1-4* cells grown in YPD at 23°C for 5 days to reach stationary phase (optical density at 600 nm = 10) were found to have about 80% of the population as unbudded $G_1$ cells compared to over 95% for wild-type cells (data not shown). Nevertheless, the analysis of cell morphology at various time points, after reinoculation into fresh medium and temperature shift to 37°C, confirmed the results obtained with the asynchronous culture. Moreover, it became clear from

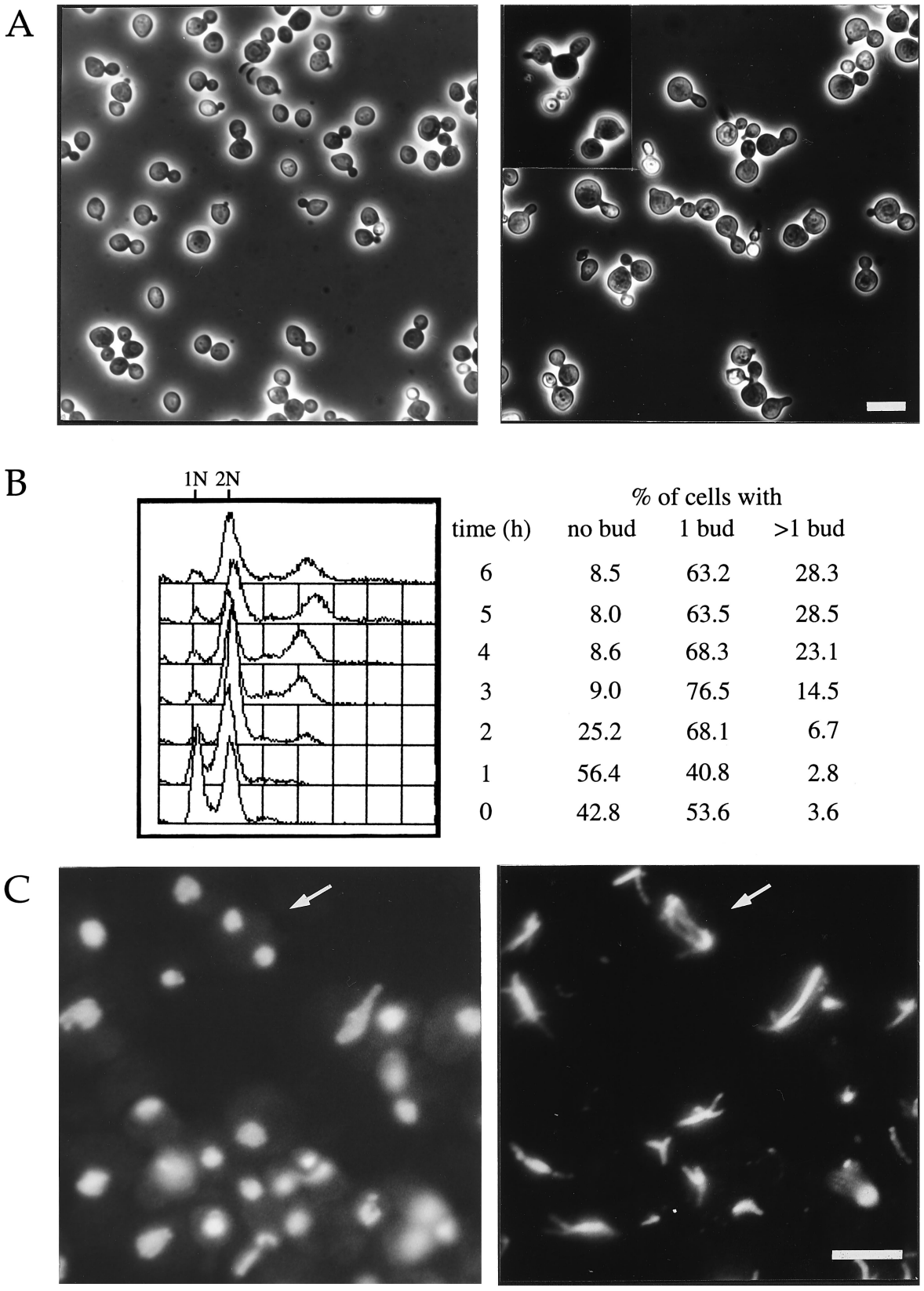


FIG. 2. Phenotypes of the *pan1-4* mutant at 37°C. An exponentially growing population of YMC387 (*pan1-4*) cells was shifted from 23 to 37°C at a density of ~1 × $10^6$ cells per ml. At the indicated intervals, cells were fixed and analyzed as described in Materials and Methods. (A) Phase-contrast micrographs illustrating the morphology of the *pan1-4* mutant at 23°C before shift (left) and after 5 h of incubation at 37°C (right). Both micrographs were taken at the same magnification. (B) Flow cytometry analysis of the *pan1-4* mutant at 37°C. The numbers on the right indicate the percentages of cells with no bud, one bud, and multiple buds. The percentages of cells and the DNA profiles did not change significantly after 6 h (data not shown). (C) Fluorescence micrographs of *pan1-4* cells stained with DAPI (left) and anti-tubulin antibody (right) after 5 h of incubation at 37°C. Each arrow indicates a cell which has just completed nuclear division within the mother cell. Bars, 8 μm.

this experiment that some cells could generate two small buds either simultaneously or in a very short interval (data not shown).

It can be summarized from these analyses that although the *pan1-4* mutation may cause rapid death and/or a colethal phenotype for cells defective in $G_1$ progression, the mutation itself apparently leads to defect or delay well after Start but unrestricted to a specific cell cycle stage.

**The *pan1-4* mutant was defective in proper organization of the actin cytoskeleton.** Screening methods similar to ours have been employed previously by others to identify genes that are required for cell viability either in Cln1- and Cln2-deficient mutants (7, 19) or in the Start-deficient *cdc28* mutants at the semipermissive temperature (41). Interestingly, genes identified this way were all found to be involved in polarized growth and cytoskeleton organization (7, 19, 41). The *pan1-4* mutant phenotypes described above, namely, the presence of binucleate cells and defects in bud growth and cytokinesis, could be attributed to abnormalities in the organization of the actin cytoskeleton (20). It is known that both astral microtubules and the actin cytoskeleton are required for proper spindle orientation and migration (46). Since the astral microtubules appeared normal in the *pan1-4* mutant (Fig. 2C), it is likely that the presence of binucleate cells could be due to perturbation in the actin cytoskeleton. On the basis of these reasons, we decided to examine the cytoskeleton distribution in *pan1-4* cells by using rhodamine-conjugated phalloidin which selectively binds to filamentous actin (16). The actin staining of wild-type cells displayed two typical structures, namely, the cortical actin patches which were highly polarized and mostly confined to the bud with little or no actin patches seen in the mother and the actin cables which were stained only in the mother and mostly aligned along the axis of bud growth (Fig. 3A). The *pan1-4* mutant grown at permissive temperature (23°C) also exhibited similar pattern of polarized cortical actin patches (Fig. 3B). However in many cells, actin cables were apparently not all aligned parallel to the mother-bud axis (Fig. 3B). The abnormality of actin structures of the *pan1-4* mutant was more thoroughly exposed when the cells were incubated at 37°C. As shown in Fig. 3C, in a striking contrast to wild-type and the *pan1-4* cells grown at 23°C, cortical actin patches in the *pan1-4* cells incubated at 37°C were not confined to the bud, and a large amount of them was retained in the mother (Fig. 3C). Many of the cortical actin patches seen in the mutant cells at 37°C were also larger in size. In addition, the actin cytoskeleton in some cells aggregated into thick cables or bars very similar to those seen in the *act1* mutants (44) but never seen in wild-type or the *pan1-4* cells grown at 23°C. The actin cables in the mother, when visible, were not arrayed orderly as in wild-type cells. It is important to note that the distribution of the actin cytoskeleton in mutant cells incubated at 37°C did not display any regular pattern in respect of bud size, suggesting that the mutant had lost its ability to reorganize the actin structure in accordance with cell cycle progression.

**The *pan1-4* mutant showed abnormal chitin deposition and budding pattern.** Defects in the actin cytoskeleton organization can lead to abnormal budding patterns and changed chitin deposition (20, 44). Yeast cells can select bud sites in one of the two distinct spatial patterns: axial for haploid **a** and α cells and bipolar for diploid **a**/α cells (11, 12). When yeast cells bud, a ring of chitin is deposited in the cell wall at the base of the neck (14). This chitin ring remains on the mother cell as a bud scar after cell division. We decided to examine the pattern of chitin deposition in the *pan1-4* mutant by Calcofluor staining, which permits the visualization of bud scars on the cell wall and hence allows the determination of the budding pattern.

The haploid (YMC387) and homozygous diploid (YMC396) *pan1-4* mutants were processed for staining with Calcofluor after growth at 25°C to log phase and temperature shift to 37°C for 4 h. The budding patterns of YMC387 and YMC396 cells differed dramatically from their isogenic wild-type counterparts (YMW2 and YNN413) (Fig. 4). At 25°C, most of the bud scars (75%) in the wild-type haploid YMW2 cells were arranged either in a line or clustered around one pole, indicative of axial budding (Fig. 4A, left). A small population (23%) has a bipolar pattern, and only 2% have the random budding pattern. However, the *pan1-4* haploid cells displayed a significant increase in the random budding pattern (40%), while 47% were of an axial pattern and 13% were of a bipolar pattern (Fig. 4B, left). The wild-type diploid YNN413 cells had most bud scars (83%) clustered at both ends of the cell, indicative of bipolar budding (Fig. 4A, right), while 11% of the population had a unipolar pattern and 6% had a random budding pattern. In contrast, the *pan1-4* homozygous diploid mutant had 68% of the bud scars distributed randomly over their surface (Fig. 4B, right), while only 26% had a bipolar pattern and 6% had a unipolar pattern at 25°C.

At 37°C, the chitin distribution in *pan1-4* haploid cells became more delocalized. The bud scars were difficult to recognize and some cells (19%) displayed an intense staining at the tip of the bud (Fig. 4C, left). The same was true for the diploid *pan1-4* cells, in which chitin delocalization became more pronounced in both mother and daughter cells, and many cells displayed staining in patches rather than circular bud scars (Fig. 4C, right).

***pan1-4* perturbed the distribution of the actin cytoskeleton in the *cdc28* mutant.** Analysis of the *pan1-4* single mutant with phalloidin and Calcofluor suggested that the mutant was defective in the organization of the actin cytoskeleton. We decided to investigate the cytoskeletal defects in the *cdc28-4 pan1-4* double mutant. As pointed out earlier, the *pan1-4* mutation, although it affected cell viability of the *cdc28-4* mutant dramatically, did not let the *cdc28-4* cells escape from being arrested as unbudded cells at 37°C. At 37°C, the *cdc28-4 pan1-4* double mutant was still predominately unbudded (81%), with $G_1$ DNA content (Fig. 5A and B, right), compared with 93% arrested as unbudded $G_1$ cells for the *cdc28-4* single mutant (Fig. 5A and B, left). It was also more pointed in shape than the *cdc28-4* single mutant. The fluorescence staining by phalloidin revealed striking difference between these two strains in distribution of the cortical actin cytoskeleton. Staining of the *cdc28-4* cells arrested at $G_1$ (3 h after temperature shift to 37°C) displayed a pattern of random distribution of the cortical actin patches (Fig. 5C, left), in agreement with the earlier report (37). In a sharp contrast, however, the staining of the double mutant from the culture that had been similarly incubated for 3 h at 37°C exhibited aggregated actin in most if not all of the unbudded cells (Fig. 5C, right). Furthermore, the actin was commonly seen to aggregate near or at the tip of pointed cells, similar to the polarized cortical actin patches at the pre-bud site in wild-type cells, although there were other cells that showed blocks of aggregated actin that did not situate at the tip of pointed cells. This result indicated that although the *pan1-4* mutation did not release *cdc28-4* cells from the $G_1$ state in terms of budding and DNA replication at restrictive temperature, it had made the mutant unable to arrest with randomized cortical actin cytoskeleton. Transformation of the double mutant with a single-copy plasmid carrying the wild-type *PAN1* gene (see below) resulted in cells with random distribution of actin patches identical to that seen in *cdc28-4* cells at 37°C (data not shown). It was therefore concluded that the aggregation of cortical actin patches in the double mutant

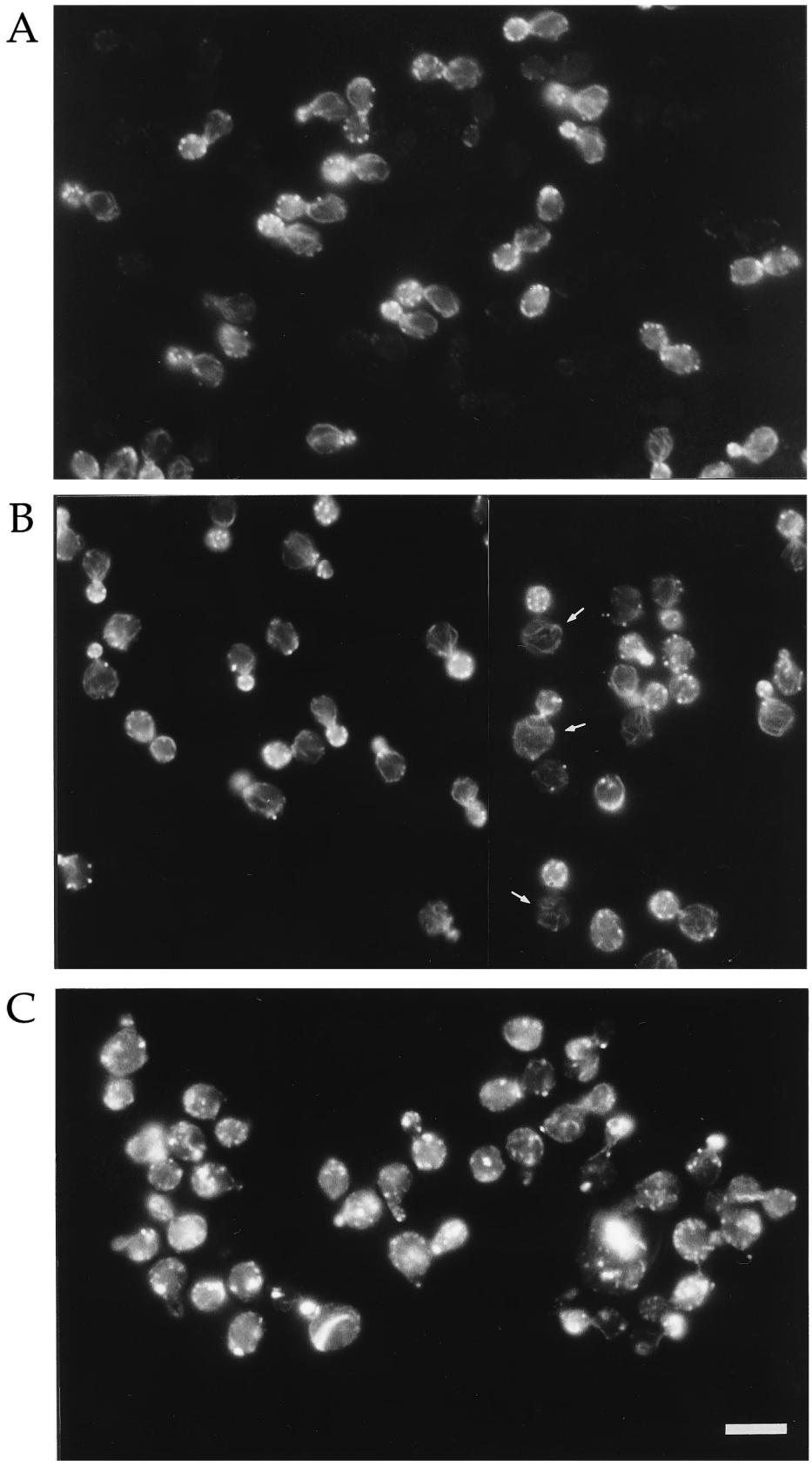


FIG. 3. Organization of the actin cytoskeleton in wild-type and *pan1-4* cells. Actin staining of exponentially growing wild-type (YMW2) cells at 30°C (A) and YMC387 (*pan1-4*) cells at 23°C (B) and then shifted to 37°C for 5 h (C) is shown. The arrows in panel B indicate cells with disoriented actin cables. Cells were fixed and stained with rhodamine-phalloidin to visualize the actin cytoskeleton as described in Materials and Methods. Bar, 8 μm.

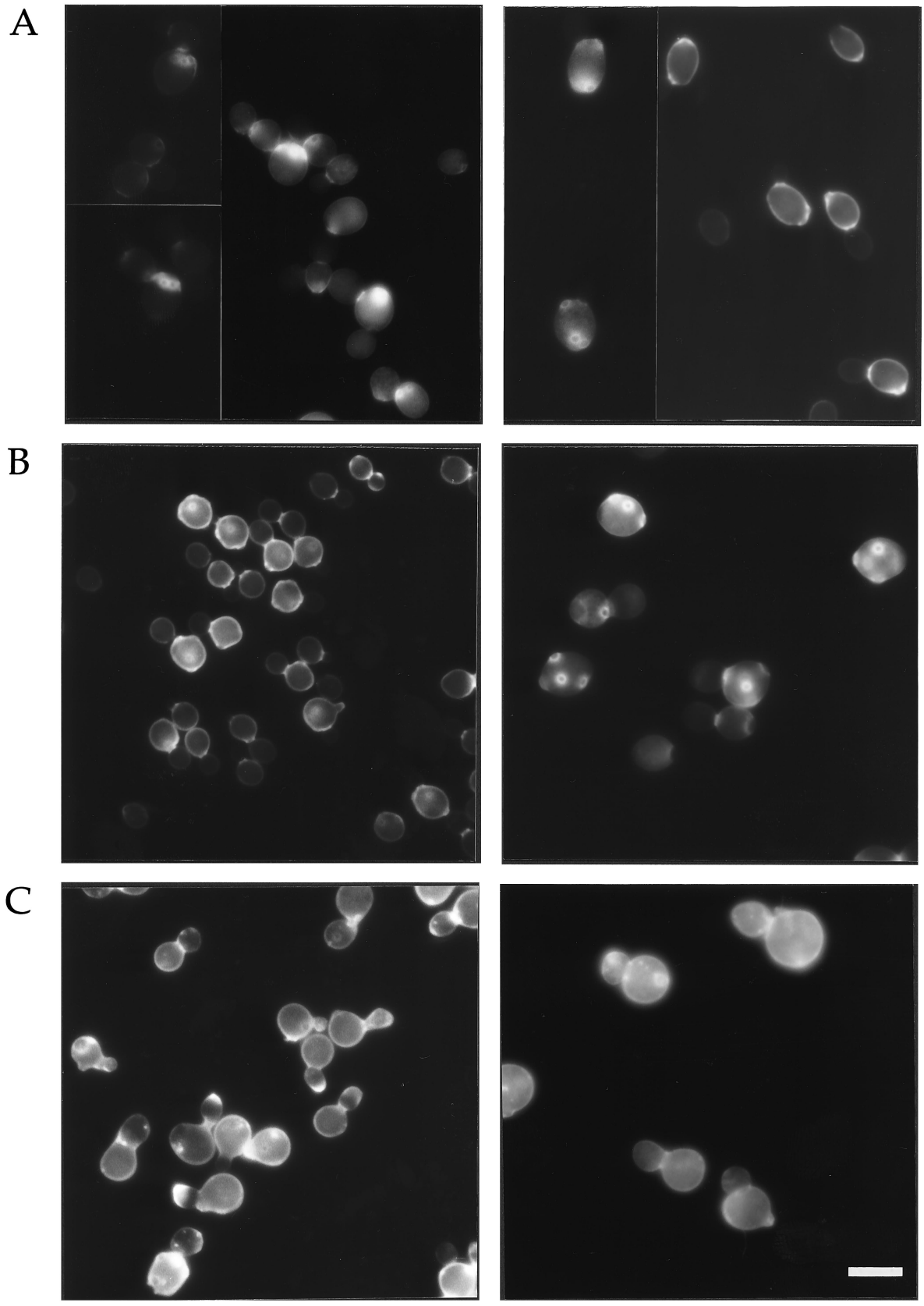


FIG. 4. Chitin and bud scar distribution in wild-type and *pan1-4* cells. Cells growing in YPD were fixed in 3.7% formaldehyde and stained for chitin with Calcofluor. (A) Wild-type YMW2 haploid (left) and YNN413 diploid (right) cells incubated at 25°C. (B) YMC387 *pan1-4* haploid (left) and YMC396 *pan1-4* diploid (right) cells incubated at 25°C. (C) YMC387 (left) and YMC396 (right) cells incubated at 37°C for 4 h. Bar, 8 μm.

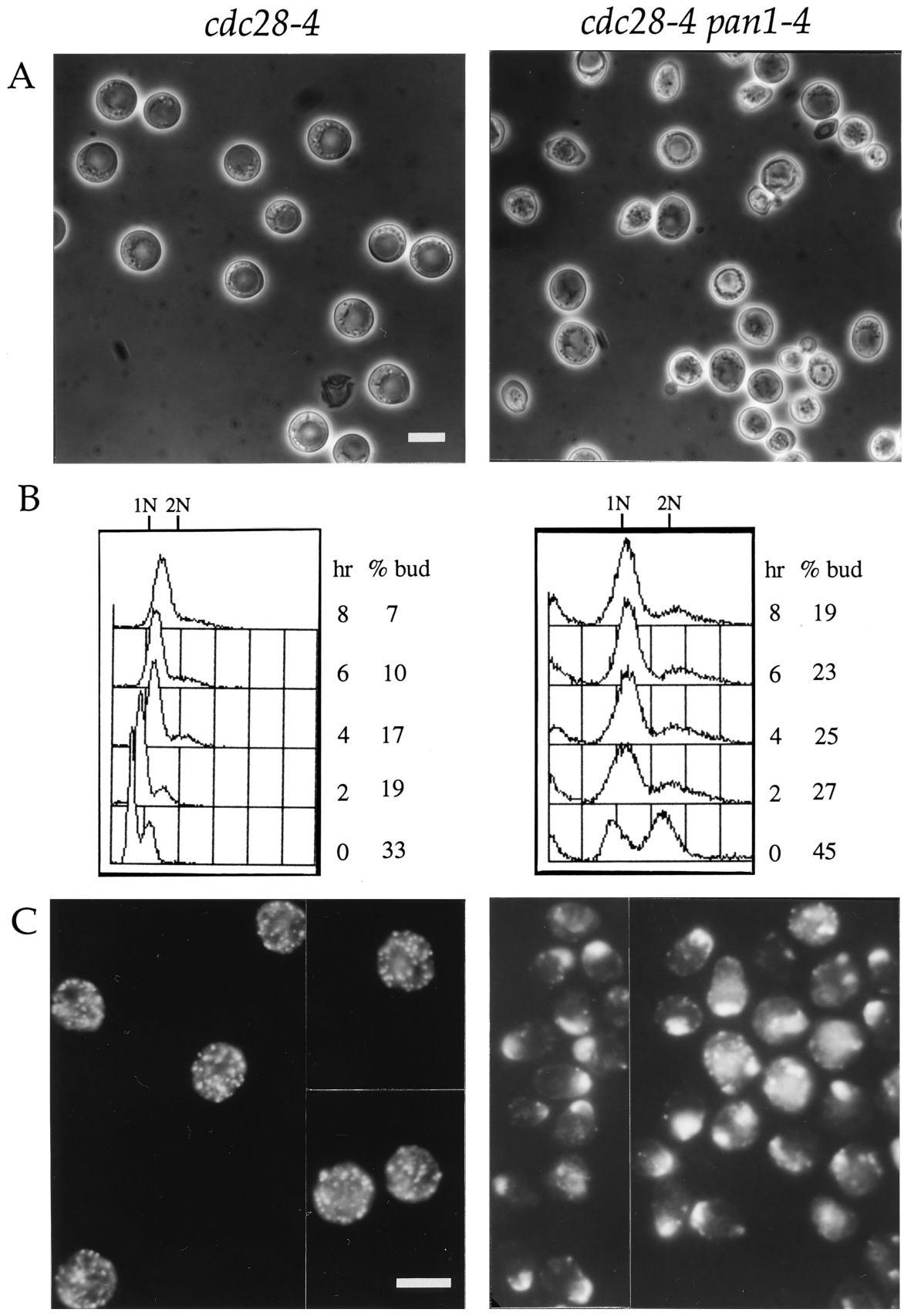


FIG. 5. Phenotypes of *cdc28-4* and *cdc28-4 pan1-4* mutants. Exponentially growing cells of US100 (*cdc28-4*) and YMC388 (*cdc28-4 pan1-4*) at 23°C were shifted to 37°C and incubated for the times indicated before fixation. (A) Phase-contrast micrographs showing the morphology of US100 (left) and YMC388 (right) strains after 3 h of incubation at 37°C. Many of the YMC388 cells are ovoid, while most of the US100 cells are round. (B) Flow cytometry analysis of US100 (left) and YMC388 (right) cells at 37°C. The rightward drift of the $G_1$ peak in US100 is a result of cell enlargement and cytoplasmic autofluorescence during each time course. (C) Fluorescence micrographs showing actin distribution in US100 (left) and YMC388 (right) after 3 h of incubation at 37°C. Cortical actin patches are dispersed in US100 and polarized in YMC388. Bars, 8 μm.

at restrictive temperature was due to the *pan1-4* mutation, not to the differences in strain background.

**Cloning and sequencing of *PAN1*.** The wild-type *PAN1* gene was cloned from a YCp50 genomic library by complementation of the *pan1-4* $Ts^-$ phenotype (Materials and Methods). One plasmid containing a 7-kb *Eco*RI fragment capable of complementation was digested with various restriction enzymes to localize the complementing gene. The smallest region of complementing activity was localized to a 2.4-kb *Eco*RI-*Pst*I fragment (Fig. 6A). DNA sequencing of this fragment revealed it to be a previously described gene named *PAN1* (52). *PAN1*, standing for poly(A) nuclease, was an essential gene and initially thought to encode a protein responsible for poly(A) tail shortening and translation initiation (52). Recently, however, it was found that the *PAN1* gene was in fact not required for the poly(A) nuclease activity (8, 52a). It had been demonstrated that only one third of the Pan1 protein was required for cell viability and a mutant protein containing deletions on both the N and C termini was also functional in a *pan1* deletion strain (52). Although the 2.4-kb *Eco*RI-PstI fragment contained the essential region of *PAN1* (Fig. 6A), it was unusual that this fragment was able to complement the *pan1-4* mutant without the *PAN1* promoter. However, many yeast genes such as *CDC44* (30) and *DBF2* (32) have also been cloned without their promoter and the N terminus. Presumably, the adjacent DNA sequences were able to provide some promoter activity needed to express these genes. Incidentally, another $Ts^-$ allele of *pan1* (*mdp3-8*) was recently reported to be complemented by a ~4-kb *Eco*RI fragment containing the *PAN1* gene without its N-terminal and promoter sequences (64).

Several lines of evidence supported the conclusion that the *pan1-4* mutation occurred in the *PAN1* gene. First, the effort to isolate the DNA sequences that were able to complement the temperature sensitivity of *pan1-4* was repeated a number of times with different yeast genomic libraries made in single-copy vectors (such as YCp50 and pRS315). Invariably, the positive clones obtained every time all contained the *PAN1* gene. Second, the *pan1-4*/*pan1*Δ::*HIS3* diploid, constructed by crossing the *pan1-4* mutant with a *pan1* deletion haploid strain kept alive by the *PAN1* gene on a plasmid, could not rescue the $Ts^-$ phenotype when the plasmid was lost (data not shown). Third, the *PAN1* gene and the *pan1-4* allele were deemed allelic to each other by the gene targeting method. The yeast *URA3* gene was targeted to the *PAN1* locus of the wild-type strain YMW1 by homologous recombination using the cloned *PAN1* sequence. One of the transformants which had the *URA3* gene correctly integrated into the *PAN1* locus (as determined by Southern hybridization) was made diploid by crossing with the *pan1-4* strain YMC387. After sporulation, tetrads were dissected and markers were analyzed. All of the 30 tetrads examined segregated as 2 $Ura^+$ $Ts^+$: 2 $Ura^-$ $Ts^-$. This demonstrated a very tight linkage between the *PAN1* locus and the original *pan1-4* mutation. These data had led us to conclude that the *pan1-4* mutation occurred in the *PAN1* gene.

The sequence of the *PAN1* gene originally published by Sachs and Deardorff contained several errors. Voss et al. recently published the nucleotide sequence of the centromeric region of yeast chromosome IX which comprised the *PAN1* locus (59). The revised *PAN1* sequence (EMBL/GenBank accession numbers Z38062 and X79743) differed from the original one in (i) a frameshift over 9 amino acids due to deletions of nucleotides 1300, 1325, and 1326 (the numbers refer to the *PAN1* sequence determined by Sachs and Deardorff); (ii) an insertion of 42 bp at 1943 resulting in addition of the peptide QTTGMMPQTTGMMP; (iii) an insertion of 15 bp at 2423 resulting in addition of the pentapeptide LNKQE; and (iv) a single base insertion at 4636 generating a frameshift over 85 amino acids in the C terminus (59). These changes in the *PAN1* gene sequence, confirmed by our own sequencing experiments, have revealed several structural features of Pan1 which were not identified previously. As shown in Fig. 6, the insertion of the QTTGMMPQTTGMMP peptide constituted a motif that was similar to Sla1, a yeast protein controlling actin cytoskeleton assembly on the cortical membrane (29). The insertion of LNKQE peptide enabled identification of the EF-hand calcium binding motif (Fig. 6C). Both motifs were located in the essential region of Pan1 as mentioned above. The frameshift at the C terminus expanded a proline-rich domain from 70 to 170 amino acids which contained a motif matching the core sequence of SH3 domain binding site (X-P-P-X-P, where X is an aliphatic residue; see reference 47). In addition, Pan1 contained a consensus sequence for the binding of phosphatidylinositol 4,5-bisphosphate ($PIP_2$) towards the C terminus which was not affected by the sequence changes (Fig. 6B).

The sequence similarities between Pan1 and Eps15, a substrate for the mammalian epidermal growth factor receptor (EGFR) and other receptor tyrosine kinases, have already been noticed (23, 59–61). Both Pan1 and Eps15 belong to a newly identified family called the EH domain (Eps15 homology domain)-containing proteins (61). The EH domain spans 70 or so amino acids and shows 60% overall sequence conservation (Fig. 6E; also see reference 61). Pan1 contained two EH domains, both of which were located in the essential region as identified by Sachs and Deardorff. Figure 6E shows the alignment of EH domains of Pan1 with that of other EH domain-containing proteins using the correct Pan1 sequence which matched the EH domain consensus better than the incorrect sequence used by Wong et al. (61).

***PAN1* was essential for cell viability.** The diploid strain with one copy of *PAN1* deleted by the one-step gene replacement method (51) gave rise to only two viable spores per tetrad (data not shown). All of the viable spores were free of the disruption marker (*HIS3*), demonstrating that disruption of the *PAN1* gene was lethal. This result confirmed the previous report that *PAN1* is an essential gene (52). The spores that carried the *PAN1* disruption mutation could germinate but died after one or two cycles of cell division (data not shown). To examine the phenotype of the *pan1* null mutant, the above diploid containing a *PAN1* deletion (constructed in YNN413) was transformed with a yeast *URA3* centromere plasmid containing the *PAN1* gene under the control of the *GAL1* promoter (see Materials and Methods). After sporulation, $Ura^+$ and $His^+$ haploids were selected and analyzed. Unfortunately, these haploid cells were still viable on glucose medium, suggesting that some low level of *PAN1* expression was occurring. Nevertheless, these haploid cells could not grow on complete synthetic medium containing 5-FOA, indicating that they required the plasmid for viability. Therefore, the inability to turn off the expression of *PAN1* completely precluded the analysis of the null mutant phenotype.

**The *pan1-4* mutant was synthetic lethal with the *Sla1* null mutant.** The homology observed between Pan1 and Sla1 prompted us to look for any genetic interactions between these two genes. Overexpression of *SLA1* under the *GAL1* promoter could not rescue the $Ts^-$ phenotype of the *pan1-4* mutation (data not shown). We then tested to see whether these two genes were involved in a common process by looking for synthetic lethality between them. A diploid strain heterozygous for both *pan1* and *sla1* mutations (*PAN1*/*pan1-4 SLA1*/*sla1*Δ::*HIS3*) was generated by crossing the *pan1-4* mutant with the *sla1* deletion mutant (see Materials and Methods). The hap-

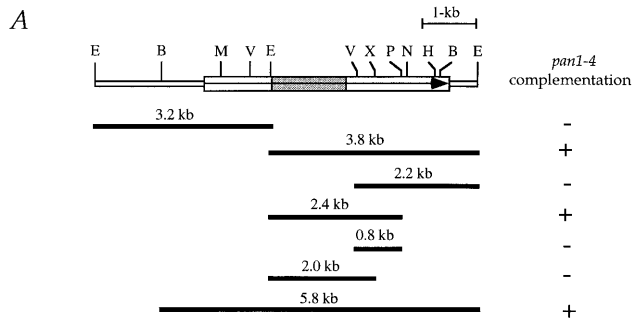


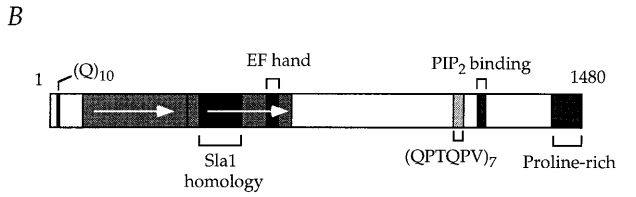


C

| | | Helix | Loop | Helix |
|---|---|---|---|---|
| Pan1 | 637 | DLEQIWNLC | DINNTGQLN | KQEFALGMHLV |
| End3 | 44 | VLNKIWFLA | DIDDDDNLD | FEEFVICMRLI |
| Calmodulin (1) | 11 | EFKEAFALF | DKDNNGSIS | SSELATVMRSL |
| Calmodulin (2) | 47 | EVNDLMNEI | DVDGNHQIE | FSEFLALMSRQ |
| Calmodulin (3) | 84 | ELLEAFKVF | DKNGDGLIS | AAELKHVLTSI |
| Fimbrin (1) | 10 | ELREAFNKI | DIDNSGYVS | DYELQDLFKEA |
| Fimbrin (2) | 50 | IIEKIFAVT | DSNKDGKIN | FEEFVSLIQEL |

D

```
Pan1     462 NITGNAL--QPQTTG--MMPQTT-GMMPQTTG--MMPQTSFGVNLGPQLTGGALQSQY
Sla1    1018 QLTGGAMMTQPQNTGSAMMPQTSFNAVPQITGGAMMPQTSFNA-L-PQVTGGAMMPLQ
              ^**  *^   ***  **   ******^    ^**  **   *******    *  **^*****^  ^
```

E

```
Eps15-eh1      GNPVYEKYYRQVDTGNTGRVLASDAAAFLKKSGLPDLILGKIWDLADTDGKGILNKQEFFVALRLV
Eps15-eh2      DKAKYDAIF-DSLSPVNGFLSGDKVKPVLLNSKLPVDILGRVWELSDIDHDGMLDRDEFAVAMFLV
Eps15-eh3      EKAKYDEIFLKTDKDMDGFVSGLEVREIFLKTGLPSTLLAHIWSLCDTKDCGKLSKDQFALAFHLI
Esp15r-eh1     GNPLYESYYKQVDPPYTGRVGASEAALFLKKSGLSDIILGKIWDLADPEGKGFLDKQGFYVALRLV
Eps15r-eh2     EKAKFDGIF-ESLLPVNGLLSGDKVKPVLMNSKLPLDVLGRVWDLSDIDKDGHLDRDEFAVAMHLV
Eps15r-eh3     DKMRFDEIFLKTDLDLDGYVSGQEVKEIFMHSGLTQNLLAHIWALADTRQTGKLSKEQFALAMYFI
Pan1-eh1       DQAKFETLFRSIVTNGSNTVSGANCRKILMRSGLPPSQLARIWTLCDTSKAGELLFPEFALAMHLI
Pan1-eh2       EKSLFYKIFETFDTQNKGLLDSPTAVEIFRKSGLNRADLEQIWNLCDINNTGQLNKQEFALGMHLV
c27F1.01c-eh1  DQAKFEQLFKSAVGREEAMSSEIG-KAILVRSKLPTVQLSKIWRLSDTTRSGRLLFPQFVLAMYLC
c27F1.01c-eh2  EKRIYDQIFDAWDKERKGTLGGNAVLEIFGQSKLTRTELEHIWNLCDHGDKGSLDRDEFAVALHLI
zk1248.3-eh1   DQAKYDSIF-QSLNPVNGKLSGAHVRPVLMNSGLDAHALARIWELSDQDKDGNLDRIEMSVALHLV
zk1248.3-eh2   NTGDYADQFAQTDTNKDGLVDGMDMRAPMMTTGLSAQILAHVWALADIKKCGQLNLEQFALTMHLL
sagA-eh        EVERYWEIF-SSLAGGQPHLNNSQAASVLRSSRLRDDQLEKVWDLADLDGDGELDFEEFCVAMRLV
YBL0520-eh1    DIAKFSQLF-DRTAKGAQTVAGDKAKDIFLKARLPNQTLGEIWALCDRDASGVLDKSEFIMAMYLI
YBL0520-eh2    KKQQFDAIFDSLDKQHAGSLSSAVLVPFFLSSRLNQETLATIWDLADIHNNAEFTKLEFALAMFLI
End3-eh        EIKKYWQIF-SGLKPIENKVNHDQVLPILYNSKLDSSVLNKIWFLADIDDDDNLDFEEFVICMRLI
                                              *    *   * * *      *    *    *
```

FIG. 6. Structure of the Pan1 protein. (A) Restriction map of the 7-kb *Eco*RI fragment containing the *PAN1* gene. The abilities of various DNA fragments, on a yeast centromere vector, to complement the $Ts^-$ phenotype of YMC387 (*pan1-4*) are indicated. All sites for *Eco*RI (E), *Bam*HI (B), *Msc*I (M), *Eco*RV (V), *Xho*I (X), *Nhe*I (N), and *Hin*dIII (H) are shown. The relevant *Pst*I (P) site is also shown. The arrow within the box represents the *PAN1* open reading frame (ORF). The stippled area represents the essential region of Pan1 identified by Sachs and Deardorff (52). (B) The Pan1 protein is composed of 1,480 instead of 1,469 amino acids as reported by Sachs and Deardorff (52). A stretch of 10 glutamine residues can be found at the N terminus (residues 13 to 22). The white arrows represent two long repeats. Only the second repeated domain is essential for viability (52). The Sla1 homology domain and the EF-hand calcium-binding domain are both located in the second long repeat. Seven repeats of the sequence QPTQPV are found in residues 1084 to 1125. The $PIP_2$-binding motif (residues 1157 to 1165 in reference 59) matches the consensus sequence found by Yu et al. (62). The proline-rich domain (residues 1310 to 1480) contains a core sequence of the SH3 domain-binding site (APPLP, residues 1360 to 1364) and an LPPP PPLP motif repeated twice (residues 1399 to 1406 and 1473 to 1480). (C) The putative EF-hand calcium-binding domain in Pan1 was compared with EF hands of End3 of *S. cerevisiae* (5), *S. cerevisiae* calmodulin (24), and chicken fimbrin (1). The EF-hand calcium-binding domain consists of two α-helices joined by a calcium-binding loop (4). (D) Sequence alignment between Pan1 and Sla1. ^, conserved changes; *, identical residues. (E) Sequence alignment of the EH domains from a variety of proteins. Generally conserved residues are highlighted, and stringently conserved residues are marked underneath (*). All sequences were retrieved from the GenBank database, with the following accession numbers: U07707 (human Eps15), U29156 (mouse Eps15r), Z38062 (*S. cerevisiae* Pan1), Z69368 (*Schizosaccharomyces pombe* ORF c27F1.01c), U29244 (*Caenorhabditis elegans* ORF zk1248.3), Z50037 (*A. nidulans* sagA), X78214 (*S. cerevisiae* ORF YBL0520), and X79473 (*S. cerevisiae* End3).

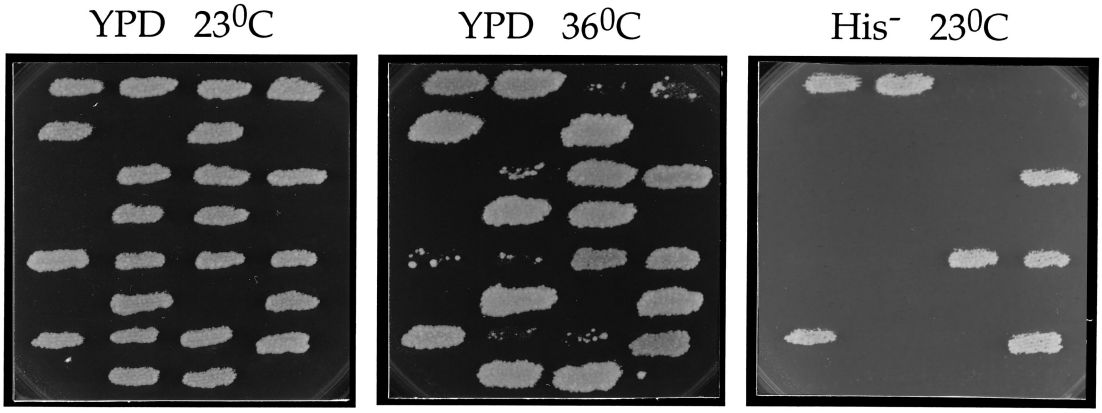


FIG. 7. Synthetic lethality between *pan1-4* and *sla1*Δ mutants at 23°C. The heterozygous diploid YMC397 (*MAT***a**/α *pan1-4*/*PAN1 sla1*Δ::*HIS3*/*SLA1*) was sporulated, dissected, and grown on a YPD plate at 23°C. Viable colonies were then patched onto a fresh YPD plate and incubated at 23°C (left). The plate was subsequently replica plated to another YPD plate incubated at 36°C (middle) and to a $His^-$ plate incubated at 23°C (right). No viable colonies were found to be both $Ts^-$ at 36°C (representing *pan1-4*) and $His^+$ at 23°C (representing *sla1*Δ).

loid *sla1* deletion mutant had a wide permissive temperature range (29). In our hands, it was temperature sensitive at 38°C but viable at 36°C and below (data not shown). The *pan1-4* mutant, on the other hand, was not viable at 36°C. Upon sporulation of the diploid at 23°C, very few tetrads with four viable spores were obtained. When all the viable spores were tested, none of them were found to exhibit both temperature sensitivity at 36°C and $His^+$ at 23°C (Fig. 7). This indicated that the *pan1-4* and *sla1* deletion mutations constituted nonconditional colethality, suggesting that these two genes may share certain functions.

**High expression of *PAN1*.** In an attempt to identify more phenotypes which may further assist the characterization of *PAN1* function, we tried overexpression of the *PAN1* gene with the inducible *GAL1* promoter. Although induction of the *GAL1*-driven *PAN1* gene carried on a centromeric vector (pMC213) did not result in obvious retardation of growth of wild-type cells (Fig. 8A), staining with anti-actin antibody revealed that high expression of *PAN1* resulted in abnormal organization of the actin cytoskeleton. As shown in Fig. 8B, pMC213-carrying cells (YMC398, Table 1) showed delocalization of the actin cytoskeleton similar to that observed in the *pan1-4* mutants incubated at restrictive temperature. This resulted in cells with a more rounded shape than the wild-type cells (Fig. 8B and 3A). Many of the cortical actin patches were also larger, and many of the cells (30%) exhibited thick actin cables which were not seen in wild-type cells. Same staining patterns were observed when rhodamine-conjugated phalloidin was used, except that the abnormal actin cables were not as apparently stained as with anti-actin antibody (data not shown). Even though a significant amount of cortical actin patches was seen in the mothers of budded cells, the buds contained more cortical actin patches than the mothers. Therefore, the cortical actin distribution was still partially under regulation throughout the cell cycle to ensure normal growth in standard culture conditions. On the other hand, the wild-type cells (YMC393) containing the *GAL1*-driven *PAN1* gene on a multicopy plasmid (pMC214) were found to be inviable in galactose medium (Fig. 8A, right).

**Cellular localization of the Pan1 protein.** To further shed light on the mechanism of *PAN1* function, the cellular localization of the Pan1 protein was determined. The *PAN1* gene expressed from its native promoter and tagged with the HA epitope (58) could not provide a sufficient amount of protein for detection with the anti-HA antibody (12CA5mAb) (data not shown). Therefore, we used the *GAL1* promoter in order to facilitate its detection. The *PAN1* gene expressed from the *GAL1* promoter in pMC213 was tagged with the HA epitope inserted immediately after the methionine initiation codon to generate pMC216. To test the expression of this construct, which was able to complement the *pan1* deletion mutation (data not shown), protein extract was made from cells carrying pMC216 and was analyzed by Western blotting. On the basis of the revised sequence of *PAN1* (59), the gene should encode a protein of 160 kDa (1,480 amino acids). However, on SDS-polyacrylamide gels, a band migrating near 200 kDa was detected (Fig. 9A, lane 2). This band was not observed from cell extract made from yeast cells carrying plasmid pMC213, which did not contain the HA tag (Fig. 9A, lane 1). In addition, two C-terminal truncated versions of HA-Pan1 were constructed and tested (see Materials and Methods). Both constructs, HA-Pan1Δ1055-1480 and HA-Pan1Δ1208-1480, displayed lower relative molecular masses when analyzed on SDS-polyacrylamide gels (Fig. 9A, lanes 3 and 4). This confirmed that the 200-kDa band was indeed HA-Pan1. This apparent discrepancy in the size of Pan1 could be attributed to its high proline content (10.1%). Abp1, which is similarly rich in proline (11.2%), has also been reported to exhibit a higher-than-calculated relative molecular mass on SDS-polyacrylamide gels (21).

To localize HA-Pan1, a yeast strain (YMC395) from which the chromosomal *PAN1* gene was deleted and which was kept alive by pMC216 was grown in galactose and prepared for immunofluorescence staining. Plasmid pMC216 had no observable effect on the viability of the cells cultured in galactose but, like pMC213, caused more delocalized cortical actin patches (Fig. 10). Using the anti-HA antibody, the Pan1 protein was found to form, or associate with, punctate structures very similar to the cortical actin patches (Fig. 10). By adjusting the focus, it was clear that these patches were localized to the plasma membrane. The staining was not exclusively confined to the membrane, and some diffusive staining was also found in the cytosol. Double immunofluorescence staining with anti-HA and anti-actin antibodies (see Materials and Methods) confirmed that the Pan1 protein was indeed associated with cortical actin patches, since both antibodies stained the same punctate structures (Fig. 10). More punctate structures could be seen from the anti-HA staining than from the anti-actin

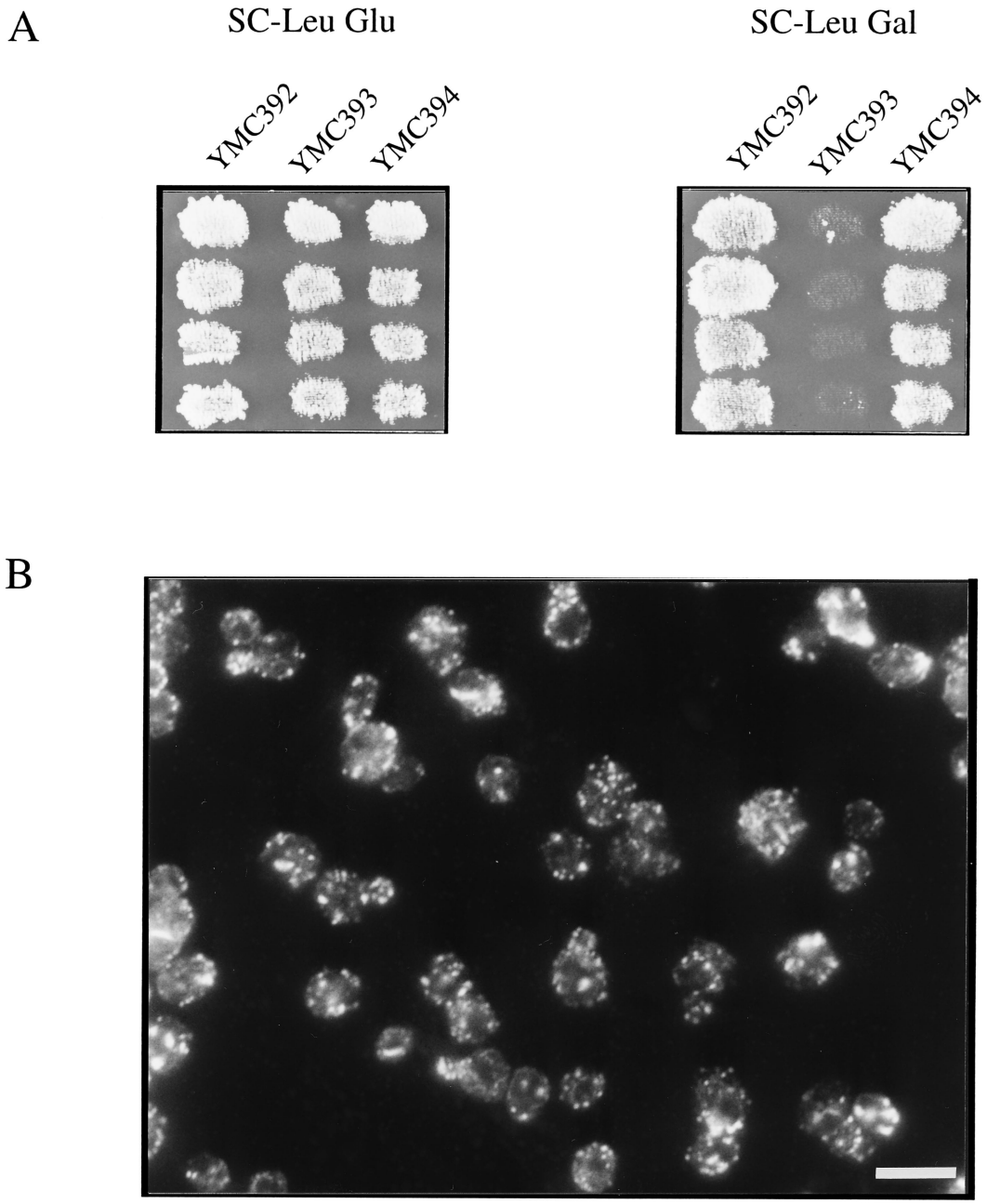


FIG. 8. Effect of *PAN1* overexpression. (A) Photographs of YMC392 (YMW2::p*GAL-PAN1 CEN6*), YMC393 (YMW2::p*GAL-PAN1* 2μm), and YMC394 (YMW2::p*GAL* 2μm) on SC-Leu glucose (left) and SC-Leu galactose (right). (B) Actin distribution in YMC398 (*pan1*Δ::p*GAL-PAN1 CEN6*). Cells grown in SC-Leu galactose at 30°C were fixed and analyzed with anti-actin antibody. Bar, 8 μm.

staining. This was probably due to the effect of overexpressing Pan1. However, most if not all of the actin patches could also be observed in the anti-HA staining. Interestingly, the Pan1 protein was found to be associated only with cortical actin patches and not with actin cables (data not shown). The staining patterns visualized with the anti-HA antibody were specific, because no staining was detected in strains without the tagged Pan1 (data not shown).

We also examined the cellular localization of the Pan1 protein by means of fractionation. Cell extracts made from YMC395 grown in galactose were subjected to centrifugation and assayed by Western blotting to see the partition of Pan1 in soluble and insoluble fractions. As shown in Fig. 9B, Pan1 was found to be present in both the supernatant and the pellet. The insoluble portion of Pan1 could not be dissociated by treatment with high pH (0.1 M $Na_2CO_3$) or 1% Triton X-100 (Fig. 9C). It, however, could be partially dissociated by 2 M urea and completely by 1% SDS (Fig. 9C). This result indicated that the Pan1 protein, when overexpressed in a tagged form, exists in two pools in the cell, soluble and membrane bound, which is consistent with our immunostaining data presented above. The latter was tightly associated with membrane (or membrane-bound structures such as the cytoskeleton) but was unlikely an integral membrane protein, again supporting the immunoflu-

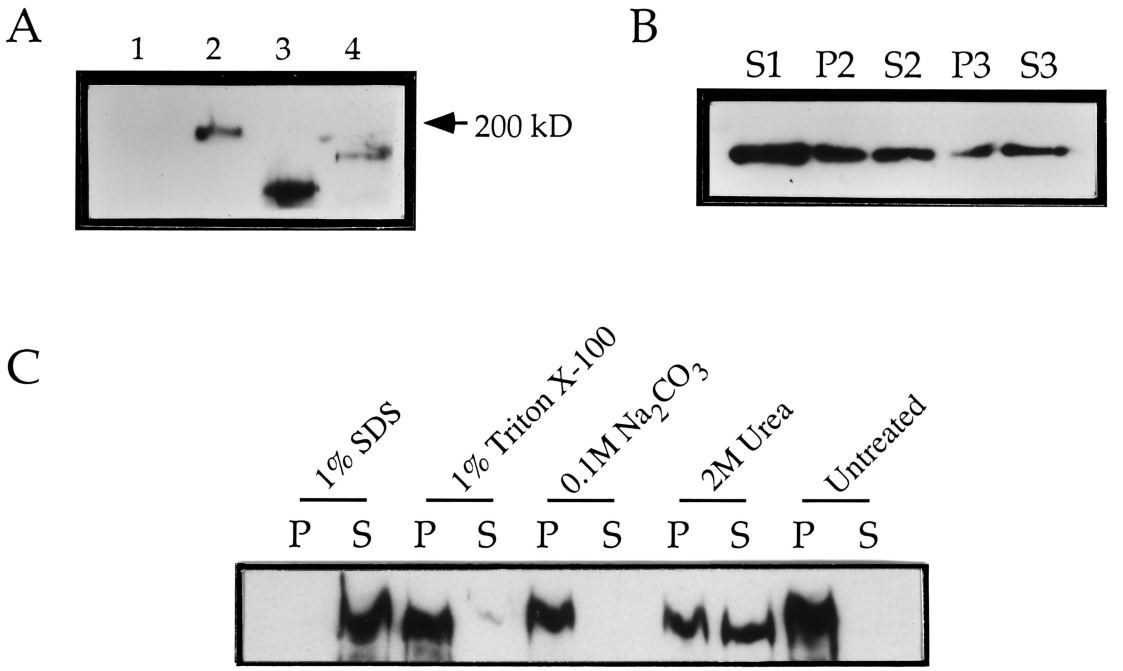


FIG. 9. Expression and fractionation of the Pan1 protein. (A) Western analysis of HA-Pan1 in crude extracts from cells containing *GAL-PAN1* (pMC213; lane 1), *GAL-HA-PAN1* (pMC216; lane 2), *GAL-HA-PAN1Δ1055-1480* (lane 3), and *GAL-HA-PAN1Δ1208-1480* (lane 4). All cells were grown in galactose-containing selective media at 30°C to log phase. (B) Cellular fractionation of Pan1. Anti-HA immunoblot analysis of samples derived from differential centrifugation of YMC395 lysate. S1, 300 × *g* supernatant; P2, 10,000 × *g* pellet; S2, 10,000 × *g* supernatant; P3, 100,000 × *g* pellet; S3, 100,000 × *g* supernatant. (C) Solubilization of Pan1 from the particulate fraction. The 10,000 × *g* pellet was resuspended in buffer and identical aliquots were treated for 60 min at 4°C with 1% SDS, 1% Triton X-100, 0.1 M $Na_2CO_3$ (pH 11), 2 M urea, and water (untreated). The samples were then spun at 10,000 × *g* to produce the pellet (P) and supernatant (S) fractions. Equivalent amounts of the supernatants and solubilized pellets were then analyzed by Western blotting with the anti-HA antibody.

orescence staining result that Pan1 was localized to cortical actin patches.

## DISCUSSION

**Actin cytoskeleton organization may contribute to the control of Start.** Start in the yeast cell cycle defines the step to initiate bud growth, DNA replication, and other events that are required for cell division. The execution of Start requires the activity of Cdc28 kinase activated by $G_1$-specific cyclins (Cln1, Cln2, and Cln3). Cln1- and Cln2-associated Cdc28 kinase is thought to be responsible for budding, while DNA replication and other events are triggered by Cdc28 in association with other types of cyclins (54). The molecular mechanism of Start control has been under intensive investigation in recent years (17). One of the approaches that were used to decipher the Start control has been the isolation of mutations that conferred a lethal phenotype either in the Start-deficient *cdc28* mutants or in the absence of *CLN1* and *CLN2* genes (7, 19, 41). This approach has proven successful in finding some new factors involved in the execution of Start. Interestingly, genes identified by this approach, such as *SLT2* (41, 63), *CLA2*/*BUD2* (7, 19), and *CLA4* (18), are all found to be required for normal organization of actin and septin cytoskeletons and bud growth. *CLA4*, encoding a Ste20-like protein kinase capable of interacting with the Rho-type GTPase Cdc42, is also involved in control of cytokinesis (18).

In order to further elucidate the mechanism of Start control, we initiated a screening process which is similar to, but not the same as, the approach described above. This method relies on the assumption that mutations that disrupt the cell cycle arrest of the Start-deficient *cdc28* mutants will likely result in rapid loss of cell viability at restrictive temperature. Hence, by screening for the rapidly dying mutants of *cdc28-4* at 37°C, it is possible to isolate mutations occurring in genes required for proper control of the Start events. Using this method, we were able to isolate *pan1-4*, which specifically conferred the rapid-death phenotype in the *cdc28-4* background. Although it was not clear why *pan1-4* made *cdc28-4* cells die rapidly at 37°C, it nevertheless did disrupt the cell cycle arrest of *cdc28-4* at 37°C in terms of the organization of the actin cytoskeleton. Such a phenotype may provide an explanation to account for the rapid death of the *cdc28-4 pan1-4* double mutant at restrictive temperature, if the abnormal aggregation of the actin cytoskeleton in the double mutant was irreversible so that the temperature down-shift could not resume the actin organization to a state capable of supporting cell proliferation. At any rate, genetic and biochemical analyses of Pan1 have led to the conclusion that *PAN1* is required for normal organization of the actin cytoskeleton (see below). Therefore, our screening method has enabled us to identify a new factor involved in polarized growth of yeast cells. This result further demonstrated the similarity between our method and the methods described above. Like *slt2*, which encodes a MAP kinase required for polarized growth (41), *pan1-4* exhibits the property of forming synthetic lethality only with the Start-deficient (*cdc28-4*), but not with the $G_2$/M-deficient (*cdc28-1N*) *cdc28* mutants. Since polarized growth, or bud formation, cannot occur without proper distribution of the actin cytoskeleton, these results together imply that the organization of the actin cytoskeleton responsible for control of polarized growth may constitute an important aspect of Start. Indeed, reorganization of the actin cytoskeleton from randomization to polarization prior to bud formation requires the activity of Cdc28 kinase (37, 38). It is

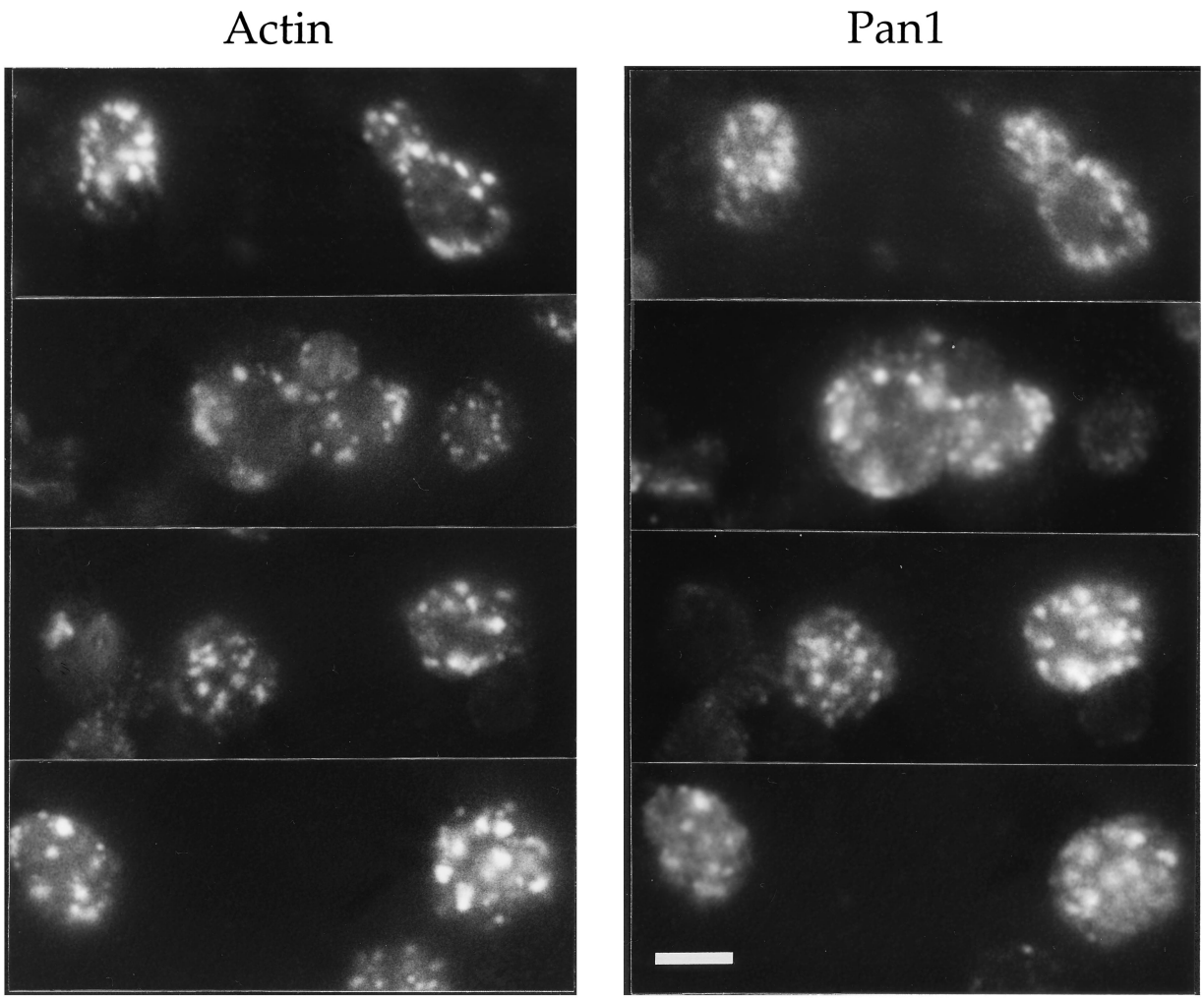


FIG. 10. Colocalization of the Pan1 protein and the cortical actin cytoskeleton. Log-phase cells of YMC395 (*pan1*Δ::p*GAL-HA-PAN1 CEN6*) grown in SC-Ura containing 2% galactose at 30°C were processed for double labelling as described in Materials and Methods. Left, indirect immunofluorescence of the actin cytoskeleton with anti-actin antibody. Right, localization of Pan1 by indirect immunofluorescence with anti-HA monoclonal antibody 12CA5. Bar, 4 μm.

reasonable to speculate that the function of the budding-related factors identified by using Start-deficient mutations may be under direct or indirect control of Cdc28. As a support for this speculation, Slt2 MAP kinase has been found recently to be partially dependent on Cdc28 for its activation (63).

***PAN1* is required for normal organization of the actin cytoskeleton.** *PAN1* was originally discovered as a gene coding for the yeast poly(A) nuclease required for initiation of translation by Sachs and Deardorff (52). Although these authors and their coworkers have reported recently that Pan1 was no longer responsible for the poly(A) nuclease activity (8, 52a), its role in initiation of translation has not yet been clarified. To test whether inhibition of protein synthesis would give rise to a phenotype similar to that of the *pan1-4* mutation, we performed the following experiments. If *pan1-4*'s phenotype was due to inhibition of protein synthesis, the *cdc28-4* mutant which we used to isolate the *pan1-4* mutation would be expected to die rapidly with aggregated actin at 37°C in the presence of cycloheximide, a drug that inhibits protein synthesis (28). However, this was not the case. The *cdc28-4* cells still showed randomized cortical actin patches at 37°C in the presence of cycloheximide and in fact survived better in the drug-containing medium at 37°C than in the normal medium (data not shown). Therefore, actin aggregation in the *cdc28* mutant in the *pan1-4* background was not the consequence of inhibition of protein synthesis. This result cast doubts on the original report that *PAN1* had an important role in initiation of translation.

Instead, our data strongly suggest that Pan1 is directly involved in the normal organization of the actin cytoskeleton. Firstly, analysis of the *pan1-4* single mutant at restrictive temperature revealed that the mutant had an abnormal actin cytoskeleton. In wild-type cells, the actin cytoskeleton showed two identifiable structures. The cortical actin patches were highly polarized, being mostly confined to the bud during the phase of bud growth, whereas the actin cables were arrayed along the mother-bud axis. In the *pan1-4* mutant, however, both structures were disturbed at nonpermissive temperature. The cortical actin patches were spread all over the mother and the daughter, and the actin cables were disarrayed from the mother-bud axis. Moreover, the mutant was no longer capable of reorganizing its cortical actin patches according to the cell cycle stages and therefore experienced lesions late in the cell cycle which might include the inability to proceed through

cytokinesis. Consistent with this notion, the actin staining of the *pan1-4* mutant at 37°C never showed congregation of actin at the mother-daughter junction, a step necessary for cytokinesis (34, 37, 38). However, the possibility that Pan1 is also directly involved in cytokinesis had not been ruled out.

Secondly, the *pan1-4* mutant showed serious defects in its budding pattern. It frequently generated two-budded cells and showed random budding patterns. Even at permissive temperature (25°C), both haploid and homozygous diploid *pan1-4* mutants demonstrated a random budding pattern as visualized with Calcofluor staining. At 37°C, the chitin distribution became delocalized and caused the whole cell surface to be brightly stained. This phenotype was in agreement with the well-established phenomenon that defects in the actin cytoskeleton organization lead to abnormal budding patterns and changed chitin deposition (3, 5, 15, 21, 25, 39, 44, 45).

Thirdly, the *pan1* mutation disrupted the pattern of actin cytoskeleton distribution in *cdc28-4* arrested cells. It has been reported that, although actin polarization in wild-type cells required the activity of Cdc28 kinase, prolonged incubation of the Start-deficient *cdc28* mutants at restrictive temperature would eventually result in polarization of the cortical actin patches (40). This phenomenon has been interpreted to be unrelated to the Start function because it happened well after the wild-type cells had formed buds (38). The *cdc28-4* mutant used in our experiments (and previously used in reference 56), however, did not polarize the actin patches during the observed time course (up to 8 h) at 37°C and remained more or less a spherical shape other than forming long projections, as seen in some *cdc28* strains (27). Nevertheless, this strain was a genuine *cdc28* mutant since the temperature sensitivity could be complemented by a copy of the wild-type *CDC28* gene (data not shown). Therefore, we attributed the discrepancy in *cdc28*-arrested morphology to the different strain background. The facts that the *pan1-4 cdc28-4* double mutant aggregated its actin patches within the first three hours at the restrictive temperature and that transformation of the double mutant with the wild-type *PAN1* gene reversed the phenotype back to randomized actin structures, as in the *cdc28-4* mutant (data not shown), suggested that *pan1-4* was solely responsible for disruption of the randomized actin distribution in the *cdc28-4* cells.

Fourthly, the *PAN1* gene sequence itself reveals some features indicative of cytoskeletal proteins. For example, there is a motif of 19 amino acids in Pan1 (MMPQTSFGVNLGPQLT GGA) that is repeated twice in another yeast protein, Sla1. While it has not been known whether the motif shared by Pan1 is important for the function of Sla1, it is located in the essential region of Pan1 (Fig. 6). *SLA1* was isolated as a synthetically lethal mutation with a null mutation of *ABP1* encoding an SH3-containing cortical actin-binding protein (29). Sla1 itself contains three SH3 domains and has been implicated in the control of cortical actin cytoskeleton assembly. At permissive temperature, the *sla1* null mutant displayed large actin spots instead of the punctate actin structures seen in wild-type cells. When shifted to the restrictive temperature, the cortical actin structures became delocalized (29). Both large actin spots and delocalization of the cortical actin structures were also observed in the *pan1-4* mutant at nonpermissive temperature, as well as in cells overexpressing the Pan1 protein. This suggests that Pan1 and Sla1 may share certain functions. In support of this, the *sla1* and *pan1-4* mutations were found to form nonconditional synthetic lethality. It is reasonable to speculate that Sla1 could interact physically with Pan1 through its SH3 domains binding to the proline-rich domain of Pan1. However, coimmunoprecipitation experiments have so far failed to demonstrate such interaction (data not shown). Another structural feature of Pan1, located also in the essential region, is the EF-hand calcium-binding domain, which is found in some other proteins implicated in organization of the actin cytoskeleton, such as End3 (5; also see below). Furthermore, Pan1 has a putative $PIP_2$-binding motif which is again a common feature found in some known actin-binding proteins such as profilin, cofilin, and gelsolin (62).

Finally, and mostly strongly, the cellular localization of the Pan1 protein suggested that Pan1 was directly involved in actin cytoskeleton organization. Using epitope-tagged Pan1, we were able to show that Pan1 was co-localized with cortical actin patches. Pan1, therefore, may be a novel actin-binding protein, although direct interaction between Pan1 and actin has yet to be demonstrated. The protein fractionation experiment also suggested that at least some fractions of the Pan1 protein were associated with membrane-bound structures, supporting the data obtained with immunofluorescence staining.

These data have led us to conclude that Pan1 is directly involved in the organization of the actin cytoskeleton. A recent report by Zoladek et al., who isolated the *pan1* mutation along with other mutations that affected the organization of the actin cytoskeleton from a screening for mutants that failed to distribute yeast subcellular proteins to their destinations, further lends support to our conclusion (64). Since the finding that *PAN1* was not responsible for poly(A) nuclease activity was not known to these authors at the publication of their report, their conclusion that both the actin cytoskeleton and mRNA 3′ ends are involved in subcellular protein distribution is apparently partially incorrect (64).

**The EH domain may define a subset of cytoskeleton-interacting proteins.** A recently identified protein motif, the EH domain, has been found in proteins from humans, mice, nematodes, and *S. cerevisiae* (61). A database search for more EH domain-containing proteins yielded one from *Schizosaccharomyces pombe* and another from the filamentous fungus *Aspergillus nidulans* (Fig. 6). The putative fission yeast gene, c27F1.01c, encodes an open reading frame whose product is about 20% identical to Pan1 in a 1,379-amino-acid overlap (data not shown). The EH domain has been reported to be involved in protein-protein interactions (61). However, its physiological function is still unknown at present. Here we propose that the EH domain may define a new family of proteins whose functions are related to, or dependent on, the actin cytoskeleton. This proposal is based on studies of three EH domain-containing proteins whose functions are at least partially known, namely, Eps15, End3, and Pan1. Both Eps15 (6) and End3 (5) are involved in clathrin-mediated endocytosis. The *END3* gene was isolated from a screen for mutants defective in endocytosis, along with other genes such as *ACT1* (encodes actin), *SAC6* (encodes fimbrin, an actin filament-bundling protein), *SLA2*/*END4*, *VRP1*, *RVS161*, and *RVS167*, all of which were involved in actin cytoskeleton organization (5, 35, 42). Interestingly, *SAC6* and *SLA2*/*END4* were independently isolated, along with *SLA1*, from a screen for mutants which formed synthetic lethality with a null mutant of *ABP1* (29). These results suggest that endocytosis is a process that requires the function of the actin cytoskeleton. Loss of the *END3* function resulted in cytoskeletal defects similar to that observed in the *pan1* mutant (5). Indeed, we have found that the *END3* gene was a multicopy suppressor of the *pan1-4* mutation (data not shown), suggesting that End3 and Pan1 interact with each other and/or play some overlapping roles in the organization of the actin cytoskeleton. There are still other EH domain-containing proteins (as shown in Fig. 6E) whose functions are completely unknown. It is tempting to speculate

that they may also function in actin cytoskeleton-dependent processes.

In summary, we have isolated *PAN1* as a new factor required for normal organization of the actin cytoskeleton in yeast cells. The genetic analysis of the mutant and cellular localization of the protein support the suggestion that *PAN1* is directly involved in controlling actin cytoskeleton organization. *PAN1* may prove important in our understanding of cellular morphogenesis and control of cell polarity in eukaryotic organisms.

## ACKNOWLEDGMENTS

We thank U. Surana for yeast strains and D. Botstein for the anti-actin antibody. We also thank F. C. Aw and P. S. Tan for general technical assistance.

This work was supported by the Singapore National Science and Technology Board.

## REFERENCES

1. **Adams, A. E. M., D. Botstein, and D. G. Drubin.** 1991. Requirement of yeast fimbrin for actin organization and morphogenesis in vivo. Nature (London) **354:**404–408.
2. **Adams, A. E. M., and J. R. Pringle.** 1984. Relationship of actin and tubulin distribution to bud growth in wild-type and morphogenetic-mutant *Saccharomyces cerevisiae*. J. Cell Biol. **98:**934–945.
3. **Amatruda, J. F., J. F. Cannon, K. Tatchell, C. Hug, and J. A. Cooper.** 1992. Disruption of the actin cytoskeleton in yeast capping protein mutants. Nature (London) **344:**352–354.
4. **Babu, Y. S., C. E. Bugg, and W. J. Cook.** 1988. Structure of calmodulin refined at 2.2 A resolution. J. Mol. Biol. **204:**191–204.
5. **Benedetti, H., S. Raths, F. Crausaz, and H. Riezman.** 1994. The *END3* gene encodes a protein that is required for the internalization step of endocytosis and for actin cytoskeleton organization in yeast. Mol. Biol. Cell **5:**1023–1037.
6. **Benmerah, A., J. Gagnon, B. Begue, B. Megarbane, A. Dautry-Varsat, and N. Cerf-Bensussan.** 1995. The tyrosine kinase substrate eps15 is constitutively associated with the plasma membrane adaptor AP-2. J. Cell Biol. **131:**1831–1838.
7. **Benton, B. K., A. H. Tinkelenberg, D. Jean, S. D. Plump, and F. R. Cross.** 1993. Genetic analysis of Cln/Cdc28 regulation of cell morphogenesis in budding yeast. EMBO J. **12:**5267–5275.
8. **Boeck, R., S. Tarun, Jr., M. Rieger, J. A. Deardorff, S. Muller-Auer, and A. B. Sachs.** 1996. The yeast Pan2 protein is required for poly(A)-binding protein-stimulated poly(A)-nuclease activity. J. Biol. Chem. **271:**432–438.
9. **Cai, M., and R. W. Davis.** 1990. Yeast centromere binding protein CBF1, of the helix-loop-helix protein family, is required for chromosome stability and methionine prototrophy. Cell **61:**437–446.
10. **Chant, J.** 1994. Cell polarity in yeast. Trends Genet. **10:**328–333.
11. **Chant, J., and I. Herskowitz.** 1991. Genetic control of bud site selection in yeast by a set of gene products that constitute a morphogenetic pathway. Cell **65:**1203–1212.
12. **Chant, J., and J. R. Pringle.** 1995. Patterns of bud-site selection in the yeast *Saccharomyces cerevisiae*. J. Cell Biol. **129:**751–765.
13. **Christianson, T. W., R. S. Sikorski, M. Dante, J. H. Shero, and P. Hieter.** 1992. Multifunctional yeast high-copy-number shuttle vectors. Gene **110:** 119–122.
14. **Cid, V. J., A. Duran, F. D. Rey, M. P. Snyder, C. Nombela, and M. Sanchez.** 1995. Molecular basis of cell integrity and morphogenesis in *Saccharomyces cerevisiae*. Microbiol. Rev. **59:**345–386.
15. **Cleves, A. E., P. J. Novick, and V. A. Bankaitis.** 1989. Mutation in the *SAC1* gene supress defects in yeast golgi and yeast actin function. J. Cell Biol. **109:**2939–2950.
16. **Cooper, J. A.** 1987. Effects of cytochalasin and phalloidin on actin. J. Cell Biol. **105:**1473–1478.
17. **Cross, F. R.** 1995. Starting the cell cycle: what's the point? Curr. Opin. Cell Biol. **7:**790–797.
18. **Cvrckova, F., C. De Virgilio, E. Manser, J. R. Pringle, and K. Nasmyth.** 1995. Ste20-like protein kinases are required for normal localization of cell growth and for cytokinesis in budding yeast. Genes Dev. **9:**1817–1830.
19. **Cvrckova, F., and K. Nasmyth.** 1993. Yeast G1 cyclins *CLN1* and *CLN2* and a GAP-like protein have a role in bud formation. EMBO J. **12:**5277–5286.
20. **Drubin, D. G., H. D. Jones, and K. F. Wertman.** 1993. Actin structure and function: roles in mitochondrial organization and morphogenesis in budding yeast and identification of the phalloidin-binding site. Mol. Biol. Cell **4:**1277–1294.
21. **Drubin, D. G., J. Mulholland, Z. M. Zhu, and D. Botstein.** 1990. Homology of a yeast actin-binding protein to signal transduction proteins and myosin-I. Nature (London) **343:**388–390.
22. **Drubin, D. G., and W. J. Nelson.** 1996. Origins of cell polarity. Cell **84:**335–344.
23. **Fazioli, F., L. Minichiello, B. Matoškovā, W. T. Wong, and P. P. Di Fiore.** 1993. eps15, a novel tyrosine kinase substrate, exhibits transforming activity. Mol. Cell. Biol. **13:**5814–5828.
24. **Geiser, J. R., D. van Tuinen, S. E. Brockerhoff, M. M. Neff, and T. N. Davis.** 1991. Can calmodulin function without binding calcium? Cell **65:**949–959.
25. **Haarer, N. K., S. H. Lillie, A. E. M. Adams, A. E. M. Magdolen, W. Bandlow, and S. S. Brown.** 1990. Purification of profilin from *Saccharomyces cerevisiae* and analysis of profilin-deficient cells. J. Cell Biol. **110:**105–114.
26. **Harold, F. M.** 1990. To shape a cell: an inquiry into the causes of morphogenesis of microorganisms. Microbiol. Rev. **54:**381–431.
27. **Hartwell, L. H., R. K. Mortimer, J. Culotti, and M. Culotti.** 1973. Genetic control of the cell division cycle in yeast: V. Genetic analysis of *cdc* mutants. Genetics **74:**267–286.
28. **Hereford, L. M., and L. H. Hartwell.** 1973. Role of protein synthesis in the replication of yeast DNA. Nature (London) New Biol. **244:**129–131.
29. **Holtzman, D. A., S. Yang, and D. G. Drubin.** 1993. Synthetic-lethal interactions identify two novel genes, *SLA1* and *SLA2*, that control membrane cytoskeleton assembly in *Saccharomyces cerevisiae*. J. Cell Biol. **122:**635–644.
30. **Howell, E. A., M. A. McAlear, D. Rose, and C. Holm.** 1994. CDC44, a putative nucleotide-binding protein required for cell cycle progression that has homology to subunits of replication factor C. Mol. Cell. Biol. **14:**255–267.
31. **Ito, H., Y. Jukada, K. Murata, and A. Kinura.** 1983. Transformation of intact yeast cells treated with alkali cations. J. Bacteriol. **153:**163–168.
32. **Johnston, L. H., S. L. Eberly, J. W. Chapman, H. Araki, and A. Sugino.** 1990. The product of the *Saccharomyces cerevisiae* cell cycle gene *DBF2* has homology with protein kinases and is periodically expressed in the cell cycle. Mol. Cell. Biol. **10:**1358–1366.
33. **Kellogg, D. R., and A. W. Murray.** 1995. NAP1 acts with Clb2 to perform mitotic functions and to suppress polar bud growth in budding yeast. J. Cell Biol. **130:**675–685.
34. **Kilmartin, J. V., and A. E. M. Adams.** 1984. Structural rearrangements of tubulin and actin during the cell cycle of the yeast *Saccharomyces*. J. Cell Biol. **98:**922–933.
35. **Kubler, E., and H. Riezman.** 1993. Actin and fimbrin are required for the internalization step of endocytosis in yeast. EMBO J. **12:**2855–2862.
36. **Kuchler, K., H. G. Dohlman, and J. Thorner.** 1993. The a-factor transporter (*STE6* gene product) and cell polarity in the yeast *Saccharomyces cerevisiae*. J. Cell Biol. **120:**1203–1215.
37. **Lew, D. J., and S. I. Reed.** 1993. Morphogenesis in the yeast cell cycle: regulation by Cdc28 and cyclins. J. Cell Biol. **120:**1305–1320.
38. **Lew, D. J., and S. I. Reed.** 1995. Cell cycle control of morphogenesis in budding yeast. Curr. Opin. Genet. Dev. **5:**17–23.
39. **Liu, H., and A. Bretscher.** 1989. Disruption of the single tropomyosin gene in yeast results in the disappearance of actin cables from the cytoskeleton. Cell **57:**233–242.
40. **Madden, K., and M. Snyder.** 1992. Specification of sites for polarized growth in *Saccharomyces cerevisiae* and the influence of external factors on site selection. Mol. Biol. Cell **3:**1025–1035.
41. **Mazzoni, C., P. Zarzov, A. Rambourg, and C. Mann.** 1993. The *SLT2* (*MPK1*) MAP kinase homolog is involved in polarized cell growth in *Saccharomyces cerevisiae*. J. Cell Biol. **123:**1821–1833.
42. **Munn, A. L., B. J. Stevenson, M. I. Geli, and H. Riezman.** 1995. *end5*, *end6*, and *end7*: mutations that cause actin delocalization and block the internalization step of endocytosis in *Saccharomyces cerevisiae*. Mol. Biol. Cell **6:**1721–1742.
43. **Nasmyth, K.** 1993. Control of the yeast cell cycle by the Cdc28 protein kinase. Curr. Opin. Cell Biol. **5:**166–179.
44. **Novick, P., and D. Botstein.** 1985. Phenotypic analysis of temperature-sensitive yeast actin mutants. Cell **40:**405–416.
45. **Novick, P., B. C. Osmond, and D. Botstein.** 1989. Suppressors of yeast actin mutations. Genetics **121:**659–674.
46. **Palmer, R. E., D. S. Sullivan, T. Huffaker, and D. Koshland.** 1992. Role of astral microtubules and actin in spindle orientation and migration in the budding yeast, *Saccharomyces cerevisiae*. J. Cell Biol. **119:**583–593.
47. **Pawson, T.** 1995. Protein modules and signalling networks. Nature (London) **373:**573–580.
48. **Pringle, J. R., and L. H. Hartwell.** 1981. The *Saccharomyces cerevisiae* cell cycle, p. 97–142. *In* J. N. Strathern, E. W. Jones, and J. R. Broach (ed.), The molecular biology of the yeast *Saccharomyces*: life cycle and inheritance. Cold Spring Harbor Laboratory, Cold Spring Harbor, N.Y.
49. **Rose, M. D., P. Novick, J. H. Thomas, D. Botstein, and G. R. Fink.** 1987. A *Saccharomyces cerevisiae* genomic plasmid bank based on a centromere-containing shuttle vector. Gene **60:**237–243.
50. **Rose, M. D., F. Winston, and P. Hieter.** 1990. Methods in yeast genetics: a laboratory course manual. Cold Spring Harbor Laboratory Press, Cold Spring Harbor, N.Y.
51. **Rothstein, R.** 1991. Targeting, disruption, replacement, and allele rescue: integrative DNA transformation in yeast. Methods Enzymol. **194:**281–301.
52. **Sachs, A. B., and J. A. Deardorff.** 1992. Translation initiation requires the PAB-dependent poly(A) ribonuclease in yeast. Cell **70:**961–973.

52a. **Sachs, A. B., and J. A. Deardorff.** 1995. Erratum. Cell **83:**1059.

53. **Sambrook, J., E. F. Fritsch, and T. Maniatis.** 1989. Molecular cloning: a

laboratory manual, 2nd ed. Cold Spring Harbor Laboratory Press, Cold Spring Harbor, N.Y.
54. **Schwob, E., T. Bohm, M. D. Mendenhall, and K. Nasmyth.** 1994. The B-type cyclin kinase inhibitor $p40^{SIC1}$ controls the G1 to S transition in *S. cerevisiae*. Cell **79:**233–244.
55. **Sikorski, R. S., and P. Hieter.** 1989. A system of shuttle vectors and yeast host strains designed for efficient manipulation of DNA in *Saccharomyces cerevisiae*. Genetics **122:**19–27.
56. **Surana, U., H. Robitsch, C. Price, T. Schuster, I. Fitch, A. B. Futcher, and K. Nasmyth.** 1991. The role of *CDC28* and cyclins during mitosis in the budding yeast *S. cerevisiae*. Cell **65:**145–161.
57. **Thompson, D. W.** 1961. On growth and form. Abridged [J. T. Bonner (ed.)]. Cambridge University Press, London.
58. **Tyers, M., G. Tokiwa, R. Nash, and B. Futcher.** 1992. The Cln3-Cdc28 kinase complex of *S. cerevisiae* is regulated by proteolysis and phosphorylation. EMBO J. **11:**1773–1784.
59. **Voss, H., J. Tamames, C. Teodoru, A. Valencia, C. Sensen, S. Wiemann, C. Schwager, J. Zimmermann, C. Sander, and W. Ansorge.** 1995. Nucleotide sequence and analysis of the centromeric region of yeast chromosome IX. Yeast **11:**61–78.
60. **Wong, W. T., M. H. Kraus, F. Carlomagno, A. Zelano, T. Druck, C. M. Croce, K. Huebner, and P. P. Di Fiore.** 1994. The human eps15 gene, encoding a tyrosine kinase substrate, is conserved in evolution and maps to 1p31-p32. Oncogene **9:**1591–1597.
61. **Wong, W. T., C. Schumacher, A. E. Salcini, A. Romano, P. Castagnino, P. G. Pelicci, and P. P. Di Fiore.** 1995. A protein-binding domain, EH, identified in the receptor tyrosine kinase substrate Eps15 and conserved in evolution. Proc. Natl. Acad. Sci. USA **92:**9530–9534.
62. **Yu, F., H. Sun, P. A. Janmey, and H. L. Yin.** 1992. Identification of a polyphosphoinositide-binding sequence in an actin monomer-binding domain of gelsolin. J. Biol. Chem. **267:**14616–14621.
63. **Zarzov, P., C. Mazzoni, and C. Mann.** 1996. The SLT2(MPK1) MAP kinase is activated during periods of polarized cell growth in yeast. EMBO J. **15:**83–91.
64. **Zoladek, T., G. Vaduva, L. A. Hunter, M. Boguta, B. D. Go, N. C. Martin, and N. K. Hopper.** 1995. Mutations altering the mitochondrial-cytoplasmic distribution of Mod5p implicate the actin cytoskeleton and mRNA 3′ ends and/or protein synthesis in mitochondrial delivery. Mol. Cell. Biol. **15:**6884–6894.